ISSN 0255-7193

CLAY RESEARCH

Vol. 34, No. 2

December, 2015

IOS Press

Overseas distribution
IOS Press, The Netherlands

THE CLAY MINERALS SOCIETY OF INDIA
Division of Soil Science and
Agricultural Chemistry
Indian Agricultural Research Institute
New Delhi-110 012, India

Overseas subscribers may send
their queries to IOS Press, Nieuwe
Hemweg 6B, 1013 BG Amsterdam,
The Netherlands, orders@iospress.in:
URL: http://www.iospress.nl

THE CLAY MINERALS SOCIETY OF INDIA

(Registered under Act XXI of 1860)
Registration No. S/13028 of 1982

COUNCIL FOR 2014

President	:	Dr. Kunal Ghosh
Vice presidents	:	Dr. Tapas Bhattacharyya
		Dr. Nayan Ahmed
Secretary	:	Dr. Sankar Mahapatra
Joint Secretary	:	Dr. Kaushik Majumdar
		Dr. Gautam Goswami
Treasurer	:	Dr. Jaya N. Surya
Councilors	:	East zone: Dr. Swapna Mukherjee, Dr. R. L. Ram
		West zone: Dr. A.L. Pharande, Dr. Vilas Kharche
		North zone: Dr. H.S. Jassal, Dr. Pankaj Srivastava
		South zone: Dr. S.K. Ghosh Dastidar, Dr. K.S. Anil Kumar
		Central zone : Dr. S.K.Ray, Dr. Tapan Adhikari
Editors, Clay Research	:	Dr. S.C.Datta, Dr. K. M.Manjaiah
Past Presidents	:	Dr. S. K. Mukherjee, Dr. K.V Raman, Dr. S.K. Ghosh,
		Dr. D.K. Pal, Dr. Dipak Sarkar

EDITORIAL BOARD

International Consulting Editor	:	Dr. S.R. Krishnamurti Gummuluru
		Adjunct Associate Professor, CERAR, University
		of South Australia, Canada
		Dr. Sridhar Komarneni
		Adjunct Professor of Civil and Environmental
		Engineering & Editor-in-Chief, J. Porous Materials, USA

Annual Institutional Subscription Rates Inclusive of Air Mail and Handling Charges :

Subscription Rates (Year 2011)	Indian (INR)	Overseas (USD)
Print + online access	Rs. 1,800.00	$ 350.00
Online access	Rs. 600.00	$ 150.00
Print	Rs. 1,200.00	$ 200.00

All payments should be sent to **"The Clay Minerals Society of India"** Division of Soil Science and Agricultural Chemistry, I.A.R.I., New Delhi-110 012

Clay Research, Vol. 34, No. 2, pp. 59-65 (2015)

Characterization of Iron Nano Particles (Fe_2O_3) Synthesized *through* Co-precipitation and Sol-Gel Methods

R. GOBINATH, R. D. SINGH*, S. C. DATTA, S.P. DATTA AND SARVENDRA KUMAR

Division of Soil Science and Agricultural Chemistry, Indian Agricultural Research Institute (IARI), New Delhi, India.

Abstract–*The aim of this work was to compare co-precipitation and sol-gel synthesis methods to prepare hematite particles of desired sizes and their characterization by X-Ray Diffraction, Transmission Electron Microscopy, Scanning Electron Microscopy, Fourier Transform Infrared Spectroscopy and particle size analysis. The protocols involved use of Cetyal Trimethyl ammonium bromide and citric acid that provided stability to the particle and did overcome the agglomeration. Stable nano hematite particles were obtained using both the protocols. X-ray diffraction showed that the synthesised hematite particles were crystalline in nature. Crystallite sizes were between 41 and 43 nm, Transmission electron microscopy images showed individual particles in less than 100 nm but agglomerated also observed in sol-gel method. The absorption spectra too confirmed presence of Fe-O stretching by vibration band @ 546 in both the particles. Zeta potential (dispersion stability) did not vary with synthesis protocol.*

Introduction

More interest has been created towards the studies of metal nanoparticles and their oxide form in many areas of scientific field. The particles having one or more dimensions of the order of 100 nm or less are referred as nanoparticles (Huber, 2005), are considered to be the building blocks for nanotechnology. Nano particles possess novel properties referring as surface-to-volume ratio and greater surface area that increases reactivity and possible biochemical activities which received a great attention around the world. Among all oxide nano particles few of them curb attention by their an imperative role in many biological and geological processes especially forms of iron oxides viz, magnetite (Fe_3O_4), maghemite (γ-Fe_2O_3), and hematite (α-Fe_2O_3) are very important in the field of scientific technology. Iron oxide nanoparticles with appropriate surface behaviour are prepared by various methods such as wet chemical, dry processes, or biological techniques (Huber, 2005; Hasany *et al.*, 2012). Detailed comparison of methods is aiming to help researchers to choose appropriate and suitable method to synthesis of iron nano particle in a larger scale. And then chemical based synthesis methods are mostly adopted due to its low cost of production and more yield. Controlled synthesis has strong impulse to researchers by adjusting the conditions during preparation and it has been proved that particle size as well as the dispersion behaviour can be tailored by the associated factors in synthesis process (Ali *et al.*, 2016) and to make use of nanoparticles to novel applications such as to improve nutrient use efficiency (Akther *et al.*, 2013; DeRosa *et al.*, 2010).

Oxide presents in a variety of structures and offers a wide range of properties. Numbers of methods were availed for the production of Fe_2O_3,

***Corresponding Author Email :** rdsingh55@gmail.com

such as precipitation, sol-gel process; hydrothermal synthesis and mechanochemical process. For the present research, Fe_2O_3 nano particles were synthesised using chemical route by co-precipitation and sol-gel method to produce nano particles in a desired range.

Materials and Methods

Ferrous chloride tetra hydrate ($FeCl_2.4H_2O$), Ferric chloride hexa hydrate ($FeCl_3.6H_2O$), cetyl trimethylammonium bromide (CTAB) (Sigma-Aldrich) and Ar (inert gas) are used in co-precipitation method. In sol-gel mode of synthesis, involving of iron nitrate ($Fe(NO_3)_3.9H_2O$) as a precursor for reaction and citric acid (Merck, India) as ligand molecule to keep the nano particle in stable form were used.

Synthesis

Fe_2O_3 synthesis (Co-precipitation) (Fe-I)

Magnetic nano particle of hematite was synthesised *via* modified co-precipitation method. Salts of ferric chloride (0.074g) and ferrous chloride (0.190 g) were taken in a ratio of 2:1 to maintain the stoichiometric validation. Weighed salts were dissolved in double distilled water. Salts containing solution was stirred vigorously and continuously heated to 60-80° C. Whole process to be held under the environment of an argon (Ar) gas, which was to prevent the further oxidation of compound. Main objective of co-precipitation was achieved by addition of salts to precipitate; 10 mL of 2.5 M NaOH solution was injected to make solution to in the alkaline range to get precipitated. This process was continued for 30 minutes to complete the reaction. The concentration and amount of NaOH, controlled the shape and size of particle size.

$$2\,FeCl_3 + FeCl_2 + 8\,H_2O \text{ — } Fe_3O_4 + 8\,NaCl + 4\,H_2O$$

$$2\,Fe^{3+} + Fe^{2+} + 8\,OH^- \text{ ——— } Fe_3O_4 + 4\,H_2O$$

pH maintained at 10 by NaOH addition. Products being highly susceptible to environmental oxidation, then Fe_3O_4 (magnetite) transferred to hematite in the presence of O_2.

$$2\,Fe_3O_4 + O_2 \text{ ——— } 2\,Fe_2O_3$$

Sol-gel method (Fe-II)

Next to co-precipitation method, we had followed sol-gel method to prepare the hematite nanoparticles for use (Bagheri *et al.*, 2013). In this route of preparation required the nitrate salt of ferrous compound ($Fe(NO_3)_3.9H_2O$ and citric acid as a ligand molecules. Citric acid was naturally occurring and found to be present as well as secreted by plants. This preparation technique led to comprises of one phase present in the synthesised product. 200 mL of 0.1 M $Fe(NO_3)_3.9H_2O$ (Merck) was taken as precursor for synthesis and 0.2 M of gelatinous substance (citric acid) were prepared by dissolving 0.2 monohydrated citric acid (Merck) in double distilled water. Prepared iron solution was kept on adding drop wise in citric acid solution with vigorous stirring and agitation. Set up must be run at the temperature of 70° C upto gel has to be formed by the loss of water. Dried products were collected in crucible for annealation with wide range of 200-400° C to get the hematite nano particles. Here, we took 300 °C as an ideal for synthesis. After calcination, derived product was crushed by ball mill to get the desire size particles.

Characterization of nano particles

X-ray Diffraction (XRD)

Synthesised nano particles were first studied for their crystalinity and crystalline size of the synthesised particle by X-ray diffractometer (XRD). The CuKα radiation source was used for operating the system with a power of 15 kV and Kβ filter used as a background filter. Powdered nano particles were place in a sample holder and analyse the sample diffraction at 2θ angle from 3 to 50° with a scan speed of 1° min^{-1} and a scan step of 0.02°. To know the average particle size of the nano particle, Debye-Scherer equation was used for calculation:-

$D=K\lambda/(\beta \text{ Cos } \theta)$

Where, D is the diameter of the crystalline size, K is the shape factor (0.89 used as a typical value), λ is the wavelength of incident beam, β is the broadening of the diffraction line measured in radians at half of its maximum intensity (full width half maxima-FWHM) and θ is the Bragg's angle.

Transmission electron microscopy (TEM)

The shape of synthesised Fe_2O_3 was derived using transmission electron micrograph. 20 µl of suspension of nano particle was made from particles and placed on carbon coated side of grid. Thereafter, gird was washed with water for multiple times and again with 10-15 drops of double distilled water and finally stained with 2% urinyl acetate. TEM images of dried grids were obtained with a JEOL 100 kb Microscope (JEOL 1011) at 120 kv.

Scanning electron microscopy (SEM)

The scanning electron microscope was used to determine the morphological structure and measures size of the particle. The powdered samples tapped on palladium coated adhesive mat and further treated for sample preparation by kept the sample in ion sputtering device for overnight. The scanning images were obtained under different magnification and accelerating voltage.

Fourier Transform Infrared Spectra (FTIR)

Synthesised particles characterised for their functional group by FT-infra red spectrophotometer. The powdered samples were carried out by using the Bruker: ALPHA, FTIR/ ATR system (Typically 24 scans, Resolution-4cm^{-1}). Samples were scanned in the region of 4000-400 cm^{-1} with a deuterated triglycine sulphate as a detector.

Zeta potential measurement

Charge present over the nano particle was observed through the zeta potential estimator (Horiba). Known concentration suspension was ultra sonicated for 15 minutes and then determined for potential and size distribution of suspended nano particles.

Results and Discussions

X-ray diffraction (XRD)

The XRD patterns for Fe_2O_3 (Figure 1) nano particles (Fe I and Fe II) were analysed for its XRD peaks to analyse its crystalinity and size of the particle. It can be clearly seen from the figure, the X ray Diffraction peaks were obtained at 2 theta ranges of 24.10°, 33.10°, 35.60°, 40.70° and 49.40° indicating which attributed to the phases of 012, 104, 110, 113 and 024. Obtained peaks were matched with JCPDS card no. 33-664,

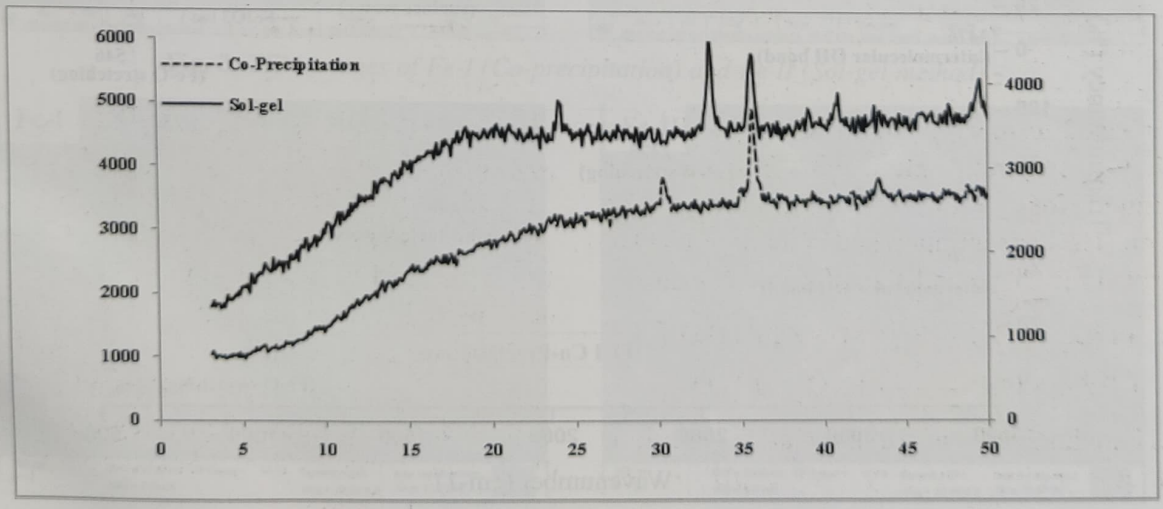

Fig. 1. *Xray diffraction pattern of Fe_2O_3 I and II*

representing that the synthesised Fe_2O_3 nanoparticles were crystalline and having the structure of hexagonal and its correspondence with results of Bagheri *et al.* (2013). Higher temperature (200- 400°C) used in synthesis causes disappearance of gamma phase; small peaks are not clearly visible to differentiate the phases. In case of co-precipitation, three peaks were observed under the angles of 30.20°, 35.60° and 43.20°. Among these peaks, intense and sharp was observed in 35.60° which is corresponding to the 110 phase, indication of FeO presence (Ghandoor *et al.* 2012). Rest of the 220 (30.20) and 202 (43.20) corresponds to the gamma phase of Fe_2O_3 present in synthesised product.

From the above peaks, two intense peaks were taken to calculate the average diameter for their confirmation. 104 and 110 were found to be the values of 43.2 nm and 43.7 nm, respectively by the Debye-Scherer equation. Changed phased noticed in this process due to influence of CTAB and citric acid, respectively. Co-precipitation(Fe-I) prepared nano particles shows two definite sharp peaks observed at 35.60.But above observed peaks are they overlapping with the findings of Sahoo *et al.* (2010). Crystalline size was intense peak was 41.7 nm. Rest of the peaks too were in a nano range but mush intense as 110 phase it might be annealing temperature causes formation of γ-Fe_2O_3 (Yen *et al.* 2002;Layek *et al.* 2010).

Scanning Electron Microscopy (SEM) &Transmission Electron Microscopy (TEM)

Morphology and size of nano particles results were observed in SEM and TEM given in figure (3 & 4). SEM images obtained from the sample indicated that most of the nano particles in the range of nano spherical with about 50-150 nm. Sample II showed aggregated and agglomerated particles and Sample I showed individual particles and not agglomerated and it is clear spherical shape crystals present in it. Agglomerated particles were present due to electrostatic force between these individual particles this might be

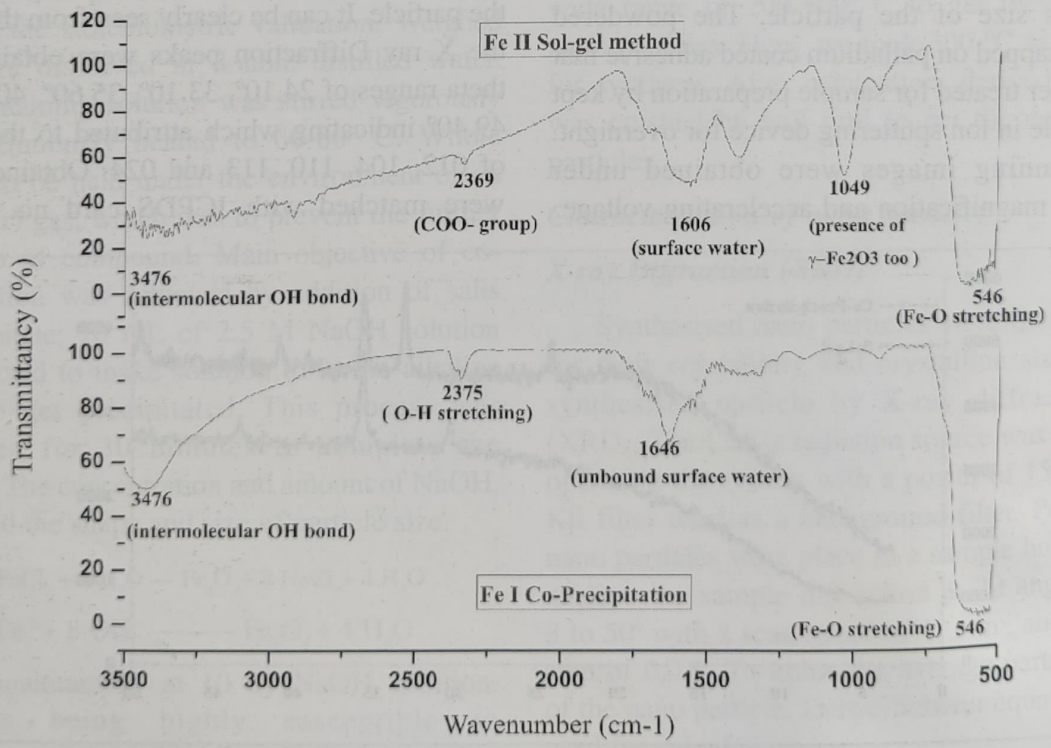

Fig. 2. *FT-IR (infra-red) pattern of hematite nano particles*

due to low concentration of CTAB added during synthesis. Morphology of hematite nano particles depended on the synthesis condition such as pH, temperature, concentration of precursor and surfactant. Agglomeration might be due to varying concentration of surfactant used during synthesis and growing of crystal (Yen *et al.* 2002). Crystallite size derived from XRD too accordance with TEM and SEM results.

FT-IR Spectroscopy

Presence of functional groups in the synthesized nano particle was determined by FT-IR spectroscopy by visible stretching and vibrational force of concerned functional group existence at room temperature. Both the methods (Figure 2) show stretching band at 546 cm^{-1} corresponds to the vibration caused by Fe-O bonds. Same piece result observed by Verdonck *et al.* (1982) and Cambier (1986), the IR band at 546-624 cm^{-1} can be assigned to Fe–O stretching vibrations. The position of this IR band was also related to the shape of goethite particles. Additional peak at 3476 cm^{-1} attributed to the hydroxyl (OH) group's presence over surface of the synthesised particles. In case Fe-I method, IR signature at 546 and 606 cm^{-1} assigned to presence of magnetite revealed that synthesis process have magnetite as a intermediate compound and too stoichiometry change during preparation. Same was observed by Ishii *et al.* (1972) and Bagheri *et al.* (2013). A peak at 1049 cm^{-1} in IR image of Fe II showed the presence of γ-Fe_2O_3 phase also in it. So, its combination of both α and γ – Fe_2O_3 in sol-gel method mediated particles over co-precipitation which comprises of pure α-Fe_2O_3 alone in it. And then in both the cases, magnetite was observed @ 606 cm^{-1}.

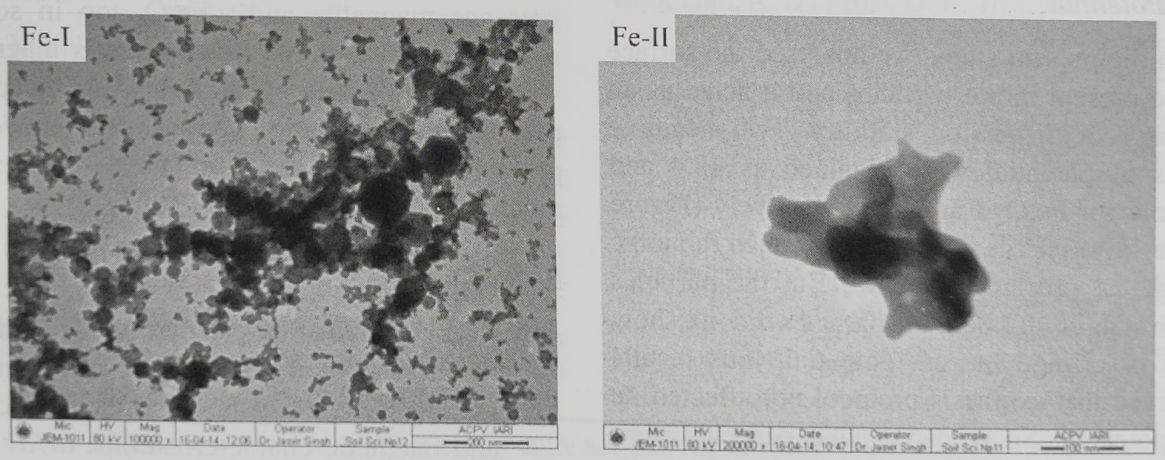

Fig. 3. *TEM images of Fe-I (Co-precipitation) and Fe II (Sol-gel method)*

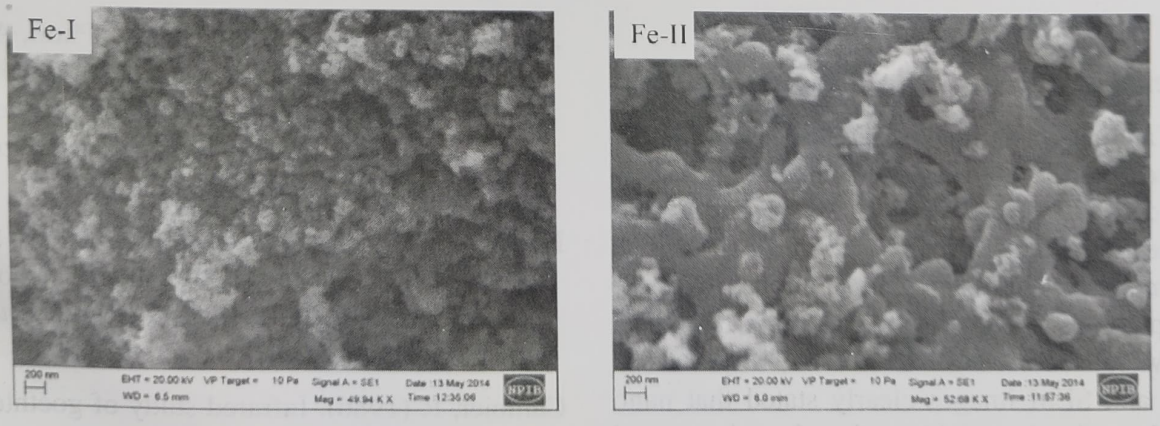

Fig. 4. *SEM images of Fe-I (Co-precipitation) and Fe II (Sol-gel method)*

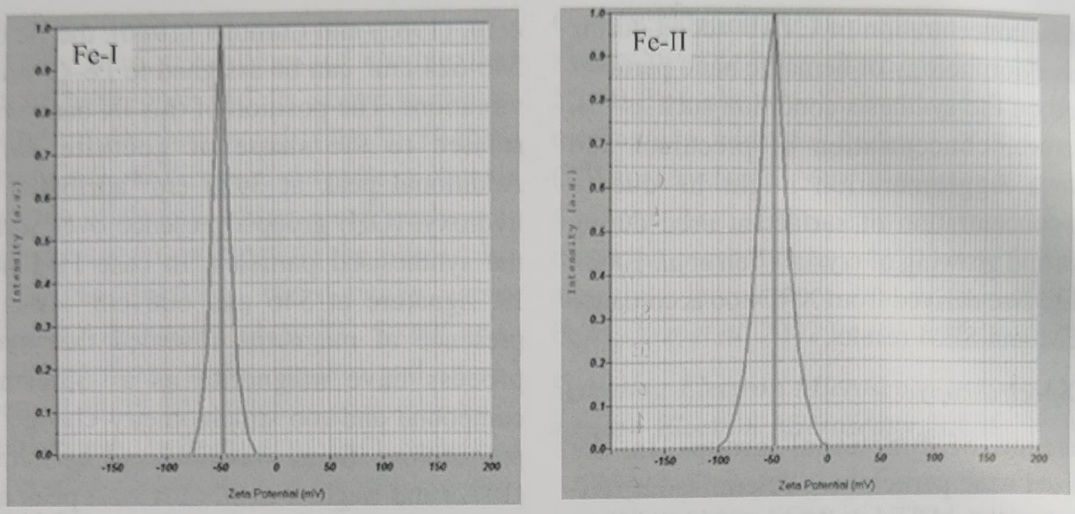

Fig. 5. *Zeta potential measurement of Fe-I (Co-precipitation) and Fe II (Sol-gel method)*

clearly mentioned that magnetite was intermediate in both the protocol to produce hematite compound (Woodland *et al.*, 2012).

Zeta Potential

In the present study, we analysed the surface charge present in the particles and it acted as an indicator of dispersion stability. Two negative values of potential were obtained as 48.4 and 49.7 mv for Fe_2O_3 I and II, respectively (Figure 5). Negative charge of particles implied the ionic strength of prepared particles. But the particles shown stability for both the particles did not show much of change in zeta potential, thus results conveyed that synthesis protocol not affected its zeta potential. So prepared nano particles were stabilized by addition of CTAB as a surfactant in it.

Conclusion

Calcination temperature used in both the procedures decided the phase formation in nano particles. XRD analysis, confirmed that synthesised nano particles showed the alpha and gamma Fe_2O_3 presence in sol-gel and co precipitation, respectively. Crystalline diameters also were in the range 43 and 42, respectively. TEM and SEM images clearly stated that nano particles sol-gel method produced agglomerated particles rather than individual particles in co-precipitation method, because of agglomeration caused by low surfactant concentration chosen in protocol. FT-IR signatures documented the presence magnetite and γ-Fe_2O_3 too in sol-gel method, because during the synthesis magnetite was the intermediate. Chemically stabilised and pure α-Fe_2O_3 (hematite) were synthesised *via* co-precipitation with desirable size over sol-gel method.

References:

Akbar, S., Hasanain, S. K., Azmat, N. and Nadeem, M. (2004). Synthesis of Fe_2O_3 nanoparticles by new Sol-Gel method and their structural and magnetic characterizations. *arXiv preprint cond-mat/0408480* .

Ali, A., Zafar, H., Zia, M., Haq, I., Phull, A. R., Ali, J. S. and Hussain, A. (2016). Synthesis, characterization, applications, and challenges of iron oxide nanoparticle. *Nanotechnology, Science and Applications,* **9**: 49-67.

Bagheri, S., Chandrappa, K. G. and Hamid, S. B. A. (2013). Generation of hematite nano particles via sol-gel method. *Research Journal of Chemical Sciences*, 3(7): 62-68.

Cambier, P. (1986). Infrared study of goethtes of varying crystalinity and particle size: II crys-

tallographic and morphological changes of synthetic goethites. *Clay Minerals*, 21: 201-210.

DeRosa, M., Monreal, C., Schnitzer, M., Walsh, R. and Sultan, Y. (2010). Nanotechnology in fertilizers. *Nature Nanotechnology*, **5**:91.

Ghandoor, H. E., Zidan, H. M., Khalil, M. M. H., and Ismail, M. I. M. (2012). Synthesis and some physical properties of magenetite nano particles. *International Journal of Elcetrochemical Science*, 7: 5734-5745.

Hasany S, Ahmed I, Rajan J, Rehman A. (2012). Systematic review of the preparation techniques of iron oxide magnetic nanoparticles. *Nanoscience and Nanotechnology*, 2(6):148–158.

Huber, D. (2005). Synthesis, properties, and applications of iron nanoparticles. *Small*, 1(5): 482-501.

Ishii, M., Nakahira, M. and Yamanaka, T. (1972). Infrared absorption spectra and cation distributions in (Mn, Fe)3O4 . *Solid State Communications*,11: 209-212.

Layek, S., Pandey, A., Pandey, A. and Verma, H. C. (2010). Synthesis of γ-Fe2O3 nanoparticles with crystallographic and magnetic texture. *International Journal of Engineering, Science and Technology*, 2(8): 33-39.

Monreal, C., DeRosa, M., Mallubhotla, S. C., Brindhaban, P.S. and Dimpka, C. (2016). Nanotechnologies for increasing the crop use efficiency of fertilizer –micronutrients. *Biology and fertility of soils*, 52:423-437.

Sahoo, S. K., Agarwal, K., Singh, A. K., Polke, B. G. and Raha, K. C. (2010). Characterization of γ- and α-Fe_2O_3 nano powders synthesized by emulsion precipitation-calcination route and rheological behaviour of á-Fe_2O_3.*International Journal of Engieering*, Science and Technology, 2(8): 118-126.en.

Verdonck, L., Hoste, S., Roelandt, F.F. and Van der Kelen, G.P. (1982) Normal coordinate analysis of or-FeOOH. A molecular approach. *Journal of Molecular Structure*, 79: 273-279.

Woodland, A. B., Frost, D. J., Trots, D. M., Klimm, K. and Mezouar, M. (2012). In situ observation of the breakdown of magnetite (Fe_3O_4) to Fe_4O_5 and hematite at high pressures and temperatures, *American Mineralogist*, 97, 1808-1811.

Yen, F. S., Chen, W. C., Yang, J. M. and Hong, C. T. (2002). Crystallite size variations of nano sized Fe_2O_3 powders during γ to α phase transformation. *Nano Letters*, 2(3): 245-252.

(Received July 2016; Accepted August 2016)

Clay Research, Vol. 34, No. 2, pp. 66-79 (2015)

Implications of Soil Clay Minerals on the Availability and Speciation of Inorganic Arsenic in Soil-crop Pathways in selected Arsenic Affected Soils of West Bengal

INDRANIL DAS*, S.K. SANYAL, K. GHOSH AND D.K. DAS

Department of Agricultural Chemistry & Soil Science, Bidhan Chandra Krishi Viswavidyalaya, Mohanpur, Nadia, West Bengal, 741252

Abstract *– Four surface soil samples three from arsenic (As)-affected soils, and one from the unaffected area of West Bengal were collected. The physical and chemical properties of the soils revealed contrasting characters. The mineralogical characterization of the corresponding clay minerals in these soils suggested the dominance of illite and kaolinite minerals. These minerals are responsible for greater As adsorption, especially the As (V) form compared to As (III). In plant body, however, As (III) predominates over As (V) though the ratio depends on the soil moisture condition. In general, there is considerable build-up of As from the As-contaminated groundwater, used as the irrigation source, to soil-plant system.*

Arsenic (As) is a ubiquitous element in the Earth's crust and is extremely toxic to humans, animals and plants. Its occurrence in natural environments may be due to natural processes (weathering reactions, biological activities and volcanic emissions) as well as anthropogenic activities (Matera and Le Hécho, 2001; Frankenberger, 2002; Mandal and Suzuky, 2002; Smedley and Kinniburgh 2002; Sanyal, 2005). Natural contamination of groundwater by As has become a crucial water quality problem in many parts of the world (Berg *et al.*, 2001; Smedley and Kinniburgh, 2002), especially in India and Bangladesh as nine districts in West Bengal, India, and 42 districts in Bangladesh have As levels in groundwater above the World Health Organization maximum permissible limit of 50 µg/L. Groundwater contamination of As has affected millions of people in these areas through its entry into the food-chain *via* groundwater-soil-plant and animal continuum.

The distribution of As in the different size-fractions of soil has been related to the stability of the primary minerals in which it is found and the extent of weathering (Huang Yan-Chu, 1994). In general, the availability of As is greater in sandy than in clay soils (Adriano, 2001), although the retention of As in clays is less efficient than that with oxides (Gräfe and Sparks, 2006). Again, As (III) adsorbs on clay minerals less intensely than does As (V). Adsorption and desorption processes that affect As mobility depends upon the structure of primary and secondary minerals retaining the As species and also the, duration of interaction. i.e., the adsorption of As (V) and As (III) by clay minerals increases with time (Lin and Puls, 2000). Zhang and Selim (2008) suggest that isomorphic substitutions of Fe by Al in clays contribute to the adsorption of As. The anionic character of As suggests that the mechanism of clay adsorption of this metalloid may be similar to that of P, through calcium-bridging mechanisms (Fixen and Grove, 1990), or else the ligand-exchange mechanism (Sanyal *et al.*, 2009). Lin and Puls (2000) found that halloysite and chlorite clays had a greater capacity to adsorb As (V) than did other clay minerals, and that kaolinite and illite/montmorillonite adsorb As (V)

***Corresponding Author Email :** dasindra@rediffmail.com; indra26july@gmail.com

to a moderate degree. Arsenic is initially adsorbed on the clay surface, but with time, it is incorporated into the structure of the mineral, forming inner-sphere complexes. The surfaces of aluminium oxides/hydroxides and clay may play a role in As adsorption, but only in acidic soils. Carbonate minerals are expected to adsorb As in calcareous soils (Sadiq, 1997; Goldberg and Glaubig, 1988).

Arsenic in groundwater is generally present as dissolved, deprotonated/protonated oxyanions, namely arsenites ($As^{III}O_3^{3-}$; $H_n As^{III}O_3^{(3-n)-}$, with n = 1, 2) or arsenate ($As^{V}O_4^{3-}$, $H_nAs^{V}O_4^{(3-n)-}$, with n = 1, 2), or both, besides the organic forms. The speciation study of the total As loading in the affected soils and the crops into arsenite and arsenate oxyanion species is important for characterising the *net* toxicity of As in the given soil-crop systems. Thus, the toxicity of arsenic compounds in groundwater/ soil environment depends largely on its oxidation state, and hence on redox status and pH, as well as whether As is present in organic combinations. The toxicity follows the order (Sanyal *et al.*, 2015):

Arsine [AsH_3; valence state of arsenic (As): +3]> organo-arsine compounds > arsenites (As^{3+}form) and oxides (As^{3+} form) > arsenates (As^{5+} form) > arsonium metals (+1)> native arsenic metal (0).

The arsenites are much more soluble, mobile and toxic than arsenates in aquatic and soil environments. The inorganic forms of As in soils and sediments include arsenites and arsenates. The organic forms, namely dimethylarsinic acid (DMA) or cacodylic acid, which on reduction (e.g., in anoxic soil conditions) forms di- and trimethyl arsines, and monomethyl arsonic acid (MMA) are also present. Under oxidizing aerobic conditions (characterized by high E_h), arsenic acid species and the arsenate oxyanions ($H_3AsO_4^0$, $H_2AsO_4^-$, $HAsO_4^{2-}$, AsO_4^{3-}) are stable in soil environment, whereas under mildly reducing conditions (such as one encounters in flooded paddy soils with E_h = 0-0.1V), and a pH range of 6 to 8, arsenous acid species and arsenite oxyanion species ($H_3As^{III}O_3^0$, $H_2As^{III}O_3^-$, $HAs^{III}O_3^{2-}$) are the stable forms (Sanyal *et al.*, 2012). Furthermore, it has been recognized that As (III) is more prevalent in soils of neutral pH range (and in most groundwater), as in the soils of the affected belt of West Bengal, India and Bangladesh, than otherwise thought, and hence is of concern. This is primarily because As (III) exists as a neutral, uncharged molecule, namely arsenous acid, $H_3As^{III}O_3^0$ (pKa= 9.2), at the pH of the neutral soils and most natural groundwater as one would expect based on the Henderson's equation (Sanyal *et al.*, 2012, 2015), and is thus less amenable to retention by the charged mineral surfaces in soils and sediments.

However, more often than not, the ratio of concentrations of arsenic species, namely the ratio, [As (III)/As (V)], in field soils does *not* quite agree with the ones computed from the observed redox potential (E_h) and the application of the Nernst's equation (at 25°C) to the equilibrium redox reaction, namely

$As^{V}O_4^{3-} + 2H^+ + 2e = As^{III}O_3^{3-} + H_2O$, and $E_h = E^0_h - 0.0295(\log [As^{III}O_3^{3-}]/[As^{V}O_4^{3-}]) - 0.059$ pH

.. (1)

The obvious reason for such deviation is that the groundwater system, subject to its withdrawal and recharge, is not, strictly speaking, a *thermodynamically* close system to which equation (1) applies. It is evident from equation (1) that the proportion of As (III), and hence soluble arsenic level in soil, should increase substantially with diminishing E_h and increasing pH. Furthermore, at a high pH, the OH^- ion concentration would increase, causing displacement of As (III) and As (V) species from their binding sites through competitive ligand-exchange reactions. There have been both direct and indirect evidence to suggest that As (and selenium) is held in soils and sediments by oxides

(e.g., of Fe, Al, Mn) through the formation of inner-sphere complexes *via* ligand-exchange mechanism (Majumdar and Sanyal, 2003). Such ligand exchange tends to increase the negative charge of the soil colloidal fraction, for instance, of iron oxides, and thus push the point of zero-charge (PZC) of the arsenic laden soil to lower pH (Sanyal *et al.*, 2009). However, the non-specific adsorption (through electrostatic mechanism) of As also occurs at pH values below the PZC for a given adsorbent. In reality, this ratio of As (V) to As (III) is only about 15-250 (Andreae, 1979), suggesting that the As (III)-As (V) couple is not in thermodynamic equilibrium, and that the ratio of As (V) to As (III) is kinetically controlled.

Masscheleyn *et al.* (1991), while examining the forms of As in a contaminated soil, reported that at relatively high redox level, lowly soluble As (V) was 65 to 98% of the soluble As level in soil at E_h = 500 mV which was 13-times more than that at E_h = - 200 mV. Douglas *et al.* (2001) reported that out of total As present in rice and vegetable crops, 95% and 5% of the compounds are present as inorganic As and organic As forms, respectively, in rice, while in vegetables, 96% and 4% of the compounds are present as inorganic As and organic As forms. Vela *et al.* (2001) extracted As species in freeze-dried carrot samples using LC-ICP-MS where they found that As (III) and As (V) are the only inorganic species present in the sample.

Keeping in view what is stated above, the present study was undertaken to find the implications of soil clay minerals on As availability in soils and reflection thereof on speciation of inorganic As in plant biomass.

Materials and Methods

Analysis of the soil properties

Four surface (0-0.15 m) composite soil samples were collected from each site of the areas namely, Nonaghata- Uttarpara (S_1 & S_2), Nonaghata-Dakshinpara (S_3) (the three soils S_1, S_2. S_3 falling in the Haringhata Block, District-Nadia of West Bengal, India, 22°27' N 88°33' E) as As-affected soils, and from Kalyani (K) (Chakdah Block, District-Nadia, West Bengal, India, 23°00' N 88°31' E) as As-unaffected area. These As affected and unaffected areas were chosen on the basis of field-level survey to assess the extent of contamination in groundwater-soil-plant and animal systems, and more specifically toxicity symptoms in humans residing in the area.

The particle-size distribution (sand, silt and clay) was determined by hydrometer method (Dewis and Freitas, 1984). pH and organic carbon of the experimental soils were analyzed according to methods described by Jackson (1973) and the exchangeable cations were measured by the procedures outlined by Sparks *et al.* (1996). The amorphous Fe/Al content of the given soils was extracted by following the methods of Saunders (1965) and Loeppert and Inskeep (1996), followed by measurement of Fe/Al by atomic absorption spectrophotometer (GBC Scientific Equipment, Australia, Model No. GBC–932B). The CEC of the soils was determined by extracting the soils with buffered $BaCl_2$ solution at a pH 8.1, adjusted with triethanolamine, by following the method described by Sumner and Miller (1996). The surface area of each soil sample was measured by the ethylene glycol retention method of Mortland and Kemper (1965). The total As was determined after digesting the soil on a sand bath with a tri-acid mixture (HNO_3: H_2SO_4: $HClO_4$:: 10 : 1 : 4, by volume). Each soil was also treated with Olsen's extractant (0.5 M $NaHCO_3$, pH 8.5) to estimate the labile As (McLaren *et al.*, 1998). The As content in the digest was measured by employing the atomic absorption spectrophotometer (AAS) coupled with hydride generator unit (GBC Scientific Equipment, Australia, HG 3000) (Huang and Fuji, 1996). The clay fractions of the selected soil samples of

the study areas were fractionated by the method described by Jackson (1973).

For the routine interpretation of the minerals present, the clay samples were Ca-saturated; Ca-glycolated; K-saturated and heated to 300 ^{0}C and 550 ^{0}C. For the semi-quantitative estimation of the clay minerals, the methodology proposed by Gjems (1967) was adopted.

Speciation of As in soils and crops

Speciation of the total As loading in the selective/representative samples in the given soils and the crops into arsenite and arsenate species was performed for characterizing the *net* toxicity of As in the given soil-crop systems by using the following principle. Prior to the speciation, the total inorganic As was extracted from the soil by using Olsen's extractant (as discussed earlier) and water. For determination of water extractable inorganic As, 2 g soil with 20 ml water was shaken for 30 minutes, followed by filtration (Tu *et al.,* 2003). For extraction of As species from plant samples, the pre-dried and crushed plant samples (10 g) were shaken with 10 mL of 50% methanol/water solution in an electronic shaker for 2 h. The samples were then centrifuged (Remi Centrifuge; Model: R-23 and R-24) at 4500 rpm for 10 min, and the supernatant was decanted into the volumetric flask. The residues were rinsed thrice by deionized water and the three extracts were combined. This method was similar to the methods outlined by Tu *et al.* (2003). Arsenate, present in the soil and plant extracts forms a blue complex with molybdate, but As (III) does not (Johnson and Pilson, 1972). This blue complex was finally measured spectrophotometrically at 840 nm wavelength by employing a digital spectrophotometer (Systronics India, Model:106). Phosphate, like As (V), also forms a blue complex with molybdate. Thus, ammonium molybdate was added to the Olsen and water extracts of the soils, as well as the plant extract for analysis of one sample aliquot which provided the concentration of As (V) plus P in the sample (Oscarson *et al.*, 1980). Then an oxidizing agent, 0.002 M iodine solution, was used for all the three extracts as above (for a second sample aliquot) which oxidized As (III) to As (V), and analysis of this treated solution provided the concentration of As (V) plus As (III) plus P. A reducing agent (mixture of sodium metabisulphite, sodium thiosulphate and sulphuric acid) was added to a third sample aliquot (of all the three extracts) which converted As (V) to As (III) and analysis of this treated solution gave the concentration of P alone (Johnson, 1971). The concentrations of As (V) and As (III) were calculated from the difference between samples 3 and 1 and that between samples 2 and 1, respectively. The crops selected for speciation study was sampled from the As affected areas, i.e., rice from Nonaghata Dakshinpara soil and mustard and weeds from Nonaghata Uttarpara soil.

Results and Discussions

Physicochemical properties of the experimental soils

Important physical and chemical properties and the Taxonomic classification of the experimental soils are given in Table 1. The soils belong to the order, Inceptisol which signifies that the soils are of recent origin in the pedogenic process. Soil pH varied from slightly acidic to neutral, ranging from 6.33 to 7.54, while the organic carbon content varied from 4.2 to 7.7 g kg^{-1}. The cation exchange capacity of these soils ranged from 16.3 to 27.6 cmol (p^+) kg^{-1} soil. Interestingly, three types of textural variations (silty clay loam, silty clay, and clay loam) were noticed in these soils where the clay content varied from 28.5 to 45.3%. The exchangeable sodium plus potassium content was highest in S_2 soil and the lowest in K soil, whereas the exchangeable calcium plus magnesium content was maximum in K soil and lowest in S_1 soil.

These variations are reflected in soil pH of these experimental soils. Amorphous iron and aluminum oxides followed the trend namely, S_3 (4.0 g kg^{-1} and 3.9 g kg^{-1})> S_2 (3.7 g kg^{-1} and 2.4 g kg^{-1}) > S_1 (3.1 g kg^{-1} and 2.1 g kg^{-1}) > K (0.19 g kg^{-1} and 0.17 g kg^{-1}). The total As content varied from 17.3 to 20.0 mg kg^{-1} in the As-affected soils and was only 3.33 mg kg^{-1} in the control site soil. The Olsen-extractable As content was relatively larger in S_3 followed by S_1, S_2 and K. Such variations in the As content may be attributed to the clay fraction, amorphous iron and aluminum content, as well as the calcium plus magnesium content of these soils.

Mineralogical characterization of the experimental soils

The semi-quantitative estimates of mineral indicated the experimental soils were dominated with illite (38.0 to 48.8%) (Table 2 & Figs. 1 to 3). However, in the control soil (K), the amount of montmorillonite (28.0%) and vermiculite (17.0%) were more compared to S_1 (13.2 and

Table 2. *Semi-quantitative mineralogical composition (%) in the clay fraction of the experimental soils*

Minerals (%)	Soils		
	S_1*	S_3*	K*
Montmorillonite	13.2	8.71	28.0
Illite	44.5	48.8	38.0
Chlorite	13.3	10.3	6.0
Vermiculite	6.25	3.55	17.0
Kaolinite	16.5	18.3	11.0
Mixed- layer	4.75	10.3	0.0

*S1 Nonaghata Uttarpara Soil (S_1) of Haringhata Block of Nadia District

S_3 Nonaghata Dakshinpara soil of Haringhata block of Nadia district

K- Kalyani soil of Chakdaha block of Nadia district (As-unaffected soil).

Table 1. *Important physicochemical properties of the experimental soils*

Parameters	Soil			
	S_1*	S_2*	S_3*	K*
Taxonomic classification	*Typic Haplustepts*			
Sand, %	19.1	15.6	9.2	41.7
Silt, %	52.4	48.2	45.5	19.6
Clay, %	28.5	36.2	45.3	38.7
pH, 1:2:5	6.33	6.74	6.82	7.54
Organic C, g/kg	4.79	4.20	7.70	4.18
Specific surface area, m^2/g	106	115	111	81
Amorphous Fe, g/kg	3.1	3.7	4.0	1.9
Amorphous Al, g/kg	2.1	2.4	3.9	1.7
CEC, cmol (p^+)/ kg	24.7	20.6	27.6	16.3
Exchangeable cations, cmol (p^+)/kg				
Na	0.09	0.16	0.10	0.09
K	0.27	0.43	0.36	0.24
Ca + Mg	7.34	8.80	11.9	12.3
Total arsenic, mg kg^{-1}	20.0	17.3	19.7	3.33
Olsen extractable As, mg kg^{-1}	4.49	3.22	4.98	0.34
Olsen extractable P, mg kg^{-1}	51.4	54.3	52.3	57.6
Total N (%)	0.091	0.042	0.098	0.064

* Soil samples, denoted by S_1, and S_2 were collected from an arsenic-affected area (namely Nonaghata Uttarpara, Haringhata Block of Nadia District) and S_3 from another arsenic-affected area (namely Nonaghata Dakshinpara, Haringhata Block of Nadia District), while the other soil sample K was collected from an arsenic-unaffected area (namely Kalyani, Chakdah Block of Nadia District).

6.25%) and S_3 (8.71 and 3.55%) soils, respectively. The kaolinite content of these soils was in the order: S_3 (18.3%) > S_1 (16.5%) > K (11.0%). Thus the As affected soils had larger illite and kaolinite content compared to K soil which had the dominance of montmorillonite and vermiculite. Indeed according to Manning and Goldberg (1996), kaolinite and illite have higher adsorption maxima for As compared to montmorillonite. In case of kaolinite, there is hardly any isomorphous substitution in either tetrahedral or octahedral layer which leads to virtual electroneutrality of these layers. Furthermore, the layers are strongly held through electrostatic hydrogen bonding which essentially leads to lower specific surface area and non-availability of interlayer spaces for As adsorption. In case of illite, the substitution of tetrahedral Si^{4+} ions by Al^{3+} ions leads to an excess negative charge which was further balanced by the interlayer monovalent or divalent cations .Because the 2:1 layers are held together more strongly in the interlayer spaces by the exchangeable cations namely, K^+, Ca^{2+}, Mg^{2+} ions, illites are non-expanding with less interlayer spaces for As adsorption. So whatever As

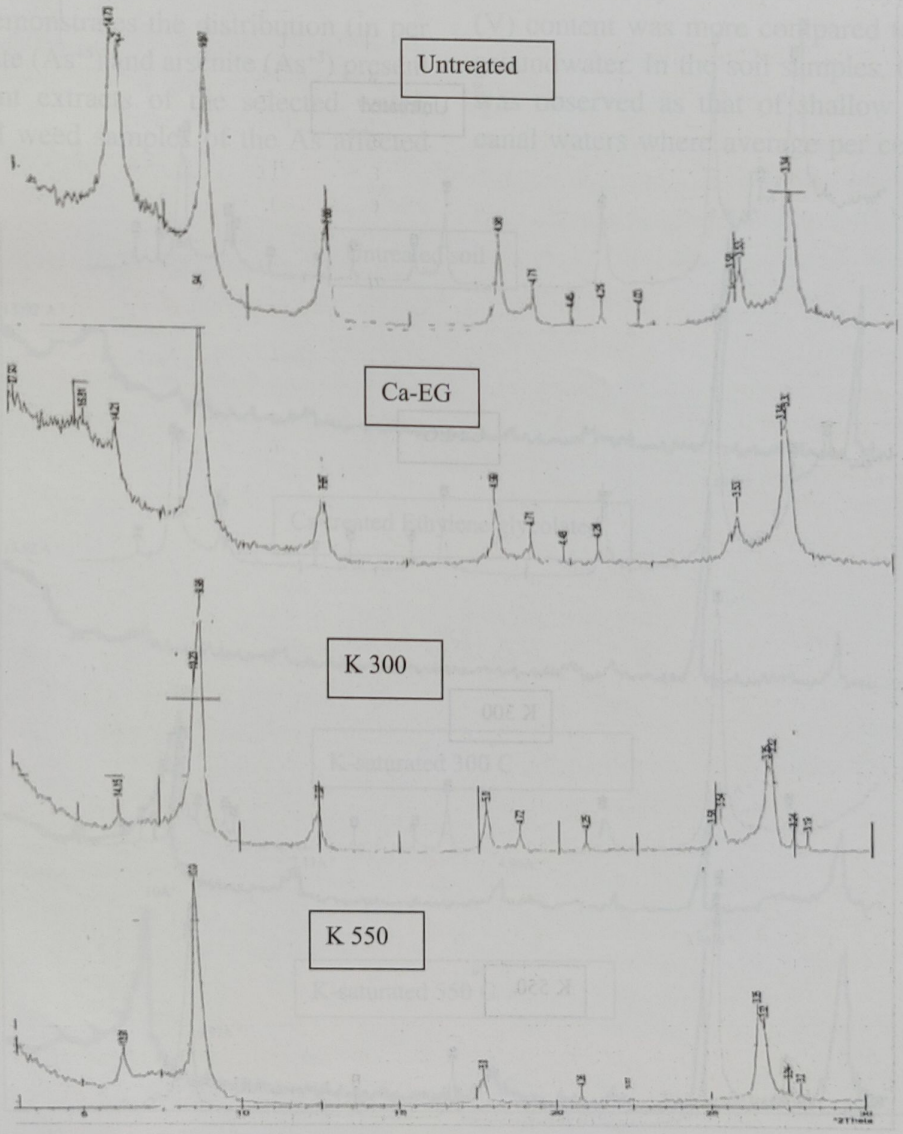

Fig. 1. *Representative X-Ray Diffractograms of clay fraction of Nonaghata Uttarpara (S_1) soil.*

adsorption takes place, it primarily depends on surface reaction. Mohapatra *et al.* (2007) reported that As (V) adsorption in clay minerals involves inner-sphere surface complexation and strong specific ion adsorption which is responsible for greater absorption in kaolinite/illite minerals. According to several workers (Muljadi *et al.*, 1966; Swartzen-Allen and Matijevic, 1974; Keren and Talpaz, 1984), the exact sites of anion adsorption on layer silicates are positively charged $(AlOH_2)^+$ functional groups at the exposed crystal edges. Huang (1975) concluded that As (V) was adsorbed on hydroxy-Al present on the external surfaces of clays, but not in the interlamellar region of vermiculite. In agreement with such earlier reports, possibility of As adsorption/retention would therefore be more in the As-affected soils with higher illite, followed by kaolinite content, as compared to K soil, which is dominated by montmorillonite and vermiculite minerals. Further, the As affected soils, especially S_1,S_2 and S_3 had higher clay, organic matter, amorphous Fe and Al content, illite-kaolinite minerals and CEC, compared to the montmorillonite-vermiculite dominated K soil. Indeed, these factors appear to be responsible

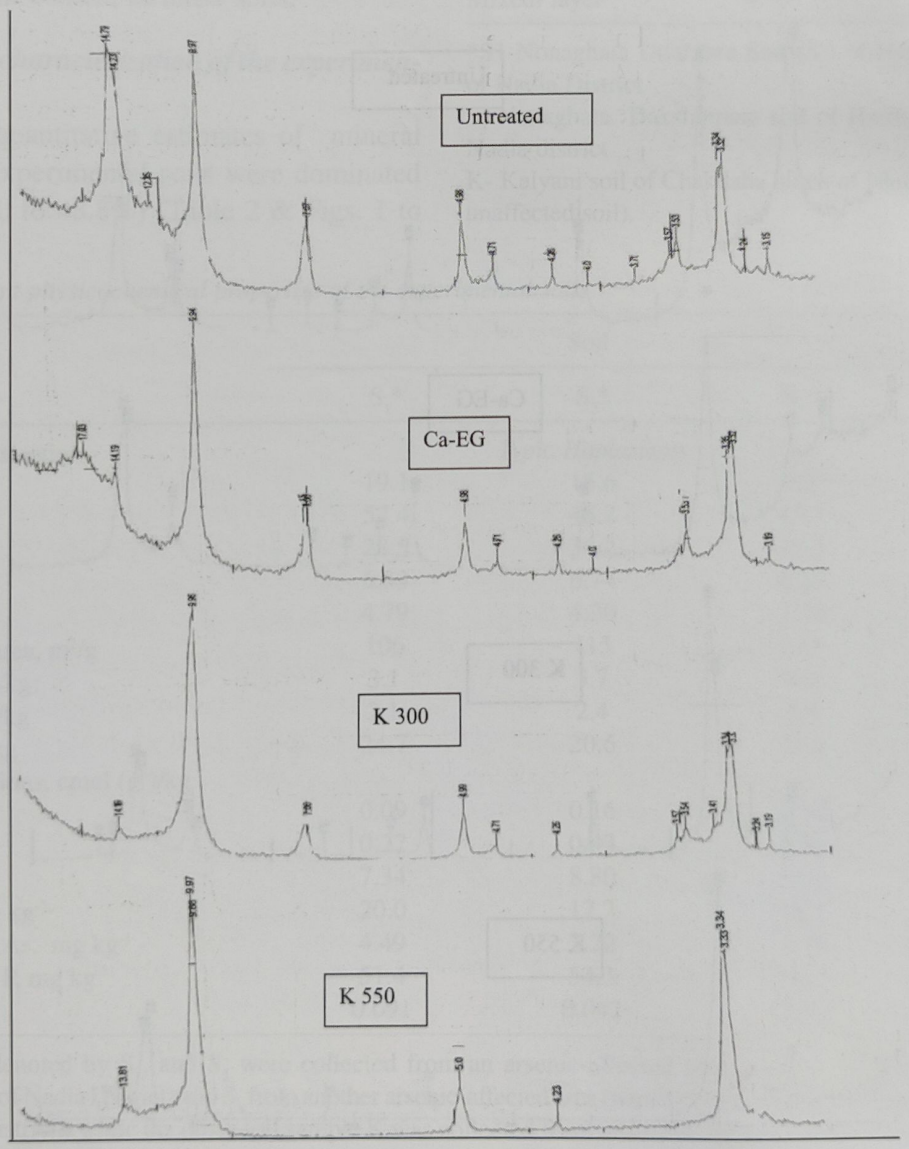

Fig. 2. *X-Ray Diffractograms of clay fraction of Nonaghata Dakshinpara (S_3) soil.*

for the given As retention behaviour of the experimental soils since a higher clay content increases the residence time of the solute to be adsorbed, while organic matter tends to complex As. The amorphous Fe and Al, on the other hand, reacts with As, forming strongly held inner-sphere adsorption complex (Goldberg *et al.*, 2001; Goldberg, 2002; Majumdar and Sanyal, 2003), whereas kaolinitic minerals facilitate As retention through inner-sphere complex formation (Mohapatra *et al.*, 2007) and non-specific adsorption.

Speciation study

Table 3 demonstrates the distribution (in per cent) of arsenate (As^{+5}) and arsenite (As^{+3}) present in the different extracts of the selected water, soil, plant and weed samples of the As affected areas. Total As loading is a crude indicator of As accumulation, which does *not* give any information as to the toxicity due to the given toxin. Hence the speciation study of inorganic As is considered essential to determine the *net* toxicity of the affected samples. In the water samples, collected from the shallow tube-wells of the affected areas (used for the irrigation purpose), the average distribution of arsenate was higher (79.1%) compared to the arsenite present (20.9%), whereas in canal water, the distribution is 92.4% arsenate and 7.6 % arsenite. The canal water being open surface water has more access to oxidation by atmospheric oxygen; hence As (V) content was more compared to the confined groundwater. In the soil samples, the same trend was observed as that of shallow tube-well and canal waters where average per cent distribution

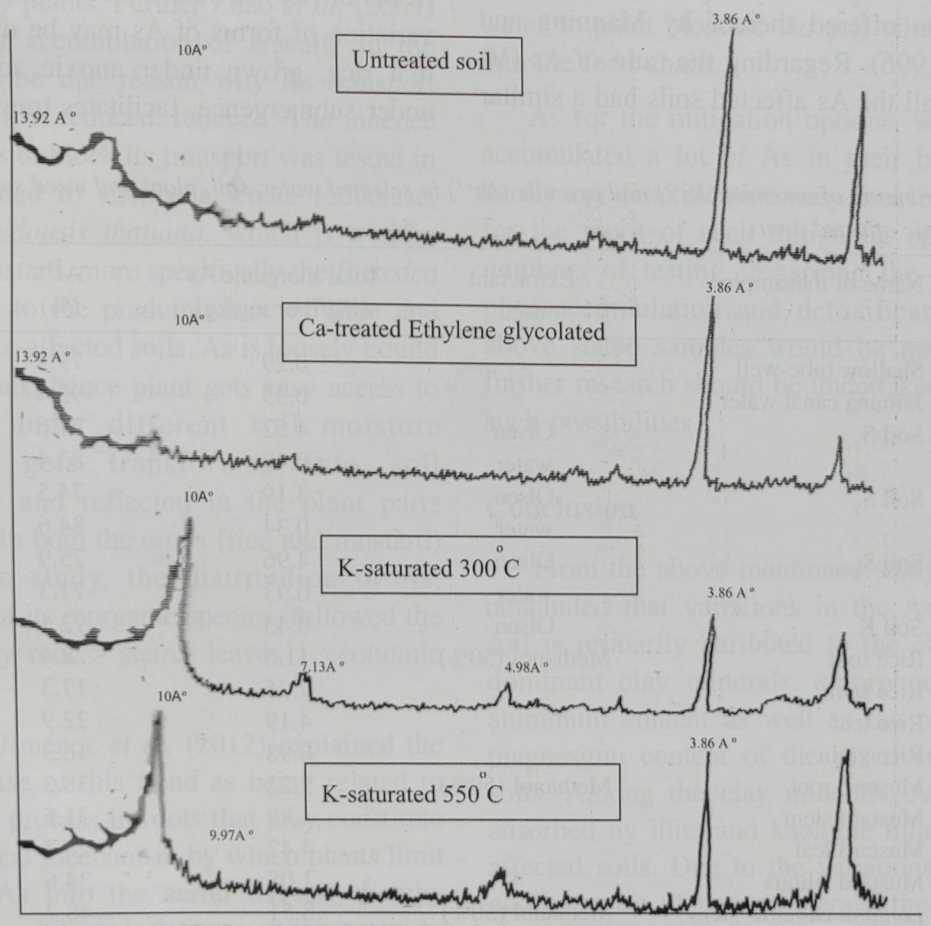

Fig. 3. *X-ray Diffractograms of clay fraction of Kalyani (K) soil.*

of arsenate was comparatively higher (77.9%). However, the total inorganic As (sum of arsenate and arsenite) content was higher in the Olsen extractant than that of the samples extracted with water. This results from the fact that the Olsen extractant facilitates solubility of As either through decreasing the concentration of Ca by high CO_3^{2-} concentration, forming $CaCO_3$, or increasing the solubility of Fe or Al arsenate as OH^- ion concentration decreases through precipitation. Similar interpretation was given by Kuo (1996) for Olsen extractant used in phosphorus extraction from soil. The higher concentration of arsenate may be attributed to the close contact of the air-water interface in these samples. Arsenate was adsorbed more by illite at a pH about 6.5. Indeed, all the experimental soils had pH close to 6.5. This was in agreement with the findings and the interpretation offered thereof by Manning and Goldberg (1996). Regarding the ratio of As (V) to As (III), all the As affected soils had a similar trend, but the K soil had comparatively lower ratio. This might be attributed to the pH and clay mineralogy of the soil as As (III) is adsorbed more at a pH about 7.0 by montmorillonite which was considerably higher in K soil compared to other soils. Similar observation was made by Frost and Griffin (1977) and Violante *et al.* (2008).

Contrary to the findings of soil and water samples, the per cent distribution of arsenite was higher in all the plant samples (extracted with methanol, 50%, w/v) examined (Table 3). This is because inside the root cells, As (V) is quickly reduced to As (III), and in many plant species, becomes complexed. The percent distribution of arsenite varied from 77.6 (roots of rice) to 61.8% (roots of mustard) in the plant samples, while the distribution of arsenate ranged from 22.4 (roots of rice) to 38.2% (roots of mustard). Such variation of forms of As may be due to the fact that rice, grown under anoxic soil conditions under submergence, facilitates transformation of

Table 3. *Distribution of arsenate (As^{+5}) and arsenite (As^{+3}) in selected water, soil, plant and weed samples collected from the arsenic affected areas*

	Name of thesample	Extractant used	Total inorganic As (mg/L or mg/kg)	As^{5+} (%)	As^{3+} (%)
Water	Shallow tube-well	-	0.29	79.1	20.9
	Jamuna canal water		0.35	92.4	7.6
Soil	Soil S_1	Olsen	4.52	77.6	22.4
		water	0.47	83.4	16.6
	Soil S_2	Olsen	3.19	74.5	25.5
		water	0.34	84.6	15.4
	Soil S_3	Olsen	4.96	75.9	24.1
		water	0.93	77.3	22.7
	Soil K	Olsen	0.43	72.1	27.9
Plant	Rice root	Methanol (50%)	11.6	22.4	77.6
	Rice stem		7.35	17.3	82.7
	Rice leaf		4.19	22.9	77.1
	Rice grain		0.98	16.3	83.7
	Mustard root	Methanol (50%)	5.22	38.2	61.8
	Mustard stem		4.89	31.5	68.5
	Mustard leaf		4.42	28.7	71.3
	Mustard siliqua		1.08	34.6	65.4
Weed	*Lantana camara* stem	Methanol (50%)	8.51	48.7	51.3
	Lantana camara leaf		10.6	42.3	57.7

arsenate (As^{5+}) to arsenite (As^{3+}) which is much more soluble and mobile (in aqueous system) and phytoextractable than the arsenate (As^{5+}) (Woolson, 1977; Sun and Doner, 1998; Sanyal, 2005), and the reflection thereto. Whereas mustard grown under upland aerobic condition accumulates As more in the arsenate than in the arsenite form, as compared to rice. Norra *et al.* (2005) reported that rice and wheat grains were not contaminated by As, but concentrations of rice roots exceeded 160 mg/kg due to Fe-rich plaque which coated the rice roots. Arsenic concentration in the uppermost soil layers of paddy fields (38 mg/kg) was little more than two times that in the soil of the less intensively watered wheat fields (18 mg/kg). Besides Moreno-Jiménez *et al.* (2012) observed that the reduction of As (V) in roots appears to be a key factor that results in blocking the xylem transport of As in many plants. Further Zhao *et al.* (2009) observed that accumulation of arsenite in the vacuole may be one reason why As transport into the xylem is reduced. reduced. The inuence of reduced As to block its transport was tested in a plant mutated to silence arsenate reductase, namely *Arabidopsis thaliana*, which is a close relative of mustard, more specifically the *Brassica* family. Due to the predominance of illite and kaolinite in As-affected soils, As is loosely bound by the minerals, hence plant gets easy access to As which, under different soil moisture conditions, gets transformed into soil differentially and reflected in the plant parts accordingly. In both the crops (rice and mustard) in the given study, the distribution of As, irrespective of its inorganic species, followed the order, namely root > stem> leaves > economic produce.

Moreno-Jiménez *et al.* (2012) explained the probable cause of this trend as being related to the reducing process in roots that may constitute a physiological mechanism by which plants limit the ow of As into the aerial tissues, thereby providing an internal defence mechanism to protect the above-ground plant biomass from the toxic effects of the metalloid. The average distribution of arsenite was also slightly higher (54.5%) than that of arsenate (46%) in the weed species examined. However, the presence of arsenite was much less compared to the edible plant samples, consumed by the humans and animals (Table 3). The increased accumulation in the aerial parts of the weed species indicates the efficacy of these weeds species to act as phytoaccumulator plants. In comparison to the crop species, the weed accumulates greater proportion of As (V) in the aerial parts. According to Moreno-Jiménez *et al.* (2012), As (V) is available for transport through the xylem in roots, presumably through the same pathways that handle phosphate in this plant.

Thus, from the table 3, it may be inferred that the *net* toxicity of the As increased from the water to plant biomass *via* soil when As enters into the food-chain.

As for the mitigation options, weed species accumulated a lot of As in their biomass, but hardly any detoxification was observed. However, for the merit of such mitigation options, large numbers of testing (regarding the capacity of phytoaccumulation and detoxification) of the above stated samples would be necessary and further research should be undertaken to explore such possibilities.

Conclusion

From the above mentioned study, it may be concluded that variations in the As content in soil is primarily attributed to the clay fraction, dominant clay minerals, amorphous iron and aluminum content as well as the calcium plus magnesium content of the given contaminated soils. Among the clay minerals, As is mainly adsorbed by illite and kaolinite minerals in As-affected soils. Due to the variations in soil pH and presence of these minerals, the ratio of As (V) to As (III) varied in these soils. Further these

minerals facilitate rather high absorption of As by plants as As is loosely bound by these minerals. The speciation of As (V) and As (III) in plant parts of the given crops was noted to depend on the soil moisture condition and the prevalent cultural practices. However, in all the plant parts, As (III) was comparatively higher compared to As (V) due to reduction of As in the plant biomass.

Acknowledgment

The financial assistance of the Indian Council of Agricultural Research, New Delhi, India during the entire course of the study is gratefully acknowledged.

References

Adriano, D.C. 2001. Trace elements in terrestrial environments. Biogeochemistry, bioavailability and risks of metals. In *Trace Elements in Tterrestrial Environments*. 2nd Edn. Springer, New York.

Andreae, M.O. 1979. Arsenic speciation in seawater and interstitial waters: the influence of biological-chemical interactions on the chemistry of a trace element. *Limnol Oceanogr.* **24 (3)**: 440–452.

Berg, M., Tran, H.C., Nguyen, T.C., Pham, H.V., Schertenleib, R. and Giger, W. 2001. Arsenic contamination of groundwater and drinking water in Vietnam: Ahuman health threat. *Environ. Sci. Technol.* **35:** 2621–2626.

Dewis, J. and Freitas, F. 1984. In: *Physical and Chemical Methods of Soil and Water Analysis.* Oxford and IBH Pub. Co., New Delhi, pp. 51-106.

Douglas, T.H., Nohora, P.V., Kristen, R.S. and Craig, S.W. 2001. Determination of total and speciated arsenic in rice by ion chromatography and ICP-MS. *J. Annl. At. Spectrom.* **16:** 299-306.

Fixen, P.E. and Grove, J.H. 1990. Testing soils for phosphorus. In (R.L. Westerman, Ed.) *Soil Testing and Plant Analysis*, 3rd Edn. Soil Science Society of America Inc., Madison, Wisconsin, USA, pp. 141–180.

Frankenberger, W.T. Jr. (Ed) 2002. *Environmental Chemistry of Arsenic*, Marcel Dekker, New York, p 391.

Frost, R.R. and Griffin, R.A. 1977. Effect of pH on adsorption of As and selenium from land fill leachate by clay minerals. *Soil Sci Soc. Am. J.* **41:** 53–57.

Gjems, O. 1967. Studies on clay minerals and clay mineral formation in soil profiles in Scandinavia. Meddelelser fra Det Norske Skogforsøkvesen, No. 81, Vol. 21. Volleberk, Norway.

Goldberg, S. and Glaubig, R.A. 1988. Anion sorption on a calcareous, montmorillonitic soil – arsenic. *Soil Sci. Soc. Am. J.* **52** (5): 1297–1300.

Goldberg, S., Lebron, I., Suarez, D.L. and Hinedi, Z.R. 2001. Surface characterization of amorphous aluminum oxides. *Soil Sci. Soc. Am. J.* **65:** 78–86.

Goldberg. S. 2002. Competitive adsorption of arsenate and arsenite on oxides and clay minerals. *Soil Sci. Soc. Am. J.* **66**: 413–421.

Gräfe, M. and Sparks, D.L. 2006. Solid phase speciation of arsenic. In (R. Naidu *et al.*, Eds.) *Managing Arsenic in the Environment. from Soils to Human Health*, CSIRO Pub, Collingwood, Australia, pp. 75–92.

Huang Yan-Chu 1994. Arsenic distribution in soils. In (J.O. Nriagu, Ed.) *Arsenic in the Environment.* Part I: Cycling and Characterization. John Wiley and Sons, Inc., New York, U.S.A., pp. 17-49.

Huang, P.M. 1975. Retention of arsenic by hydroxy-aluminum on surfaces of micaceous mineral colloids. *Soil Sci. Soc. Am. Proc.* **39**:

271–274.

Huang, P.M. and Fuji, R. 1996. Selenium and Arsenic. In (D. L. Sparks *et al.*, Eds.) *Methods of Soil Analysis*. Part 3. Chemical methods., Soil Science Society of America Inc., American Society of Agronomy Inc.: Madison, WI, USA, pp. 811–818.

Jackson, M.L. 1973. *Soil Chemical Analysis*. Prentice-Hall of India, New Delhi, pp. 326.

Johnson, D.L. 1971. Simultaneous determination of arsenate and phosphate in natural waters. *Environ. Sci. Technol.* **5:** 411-414.

Johnson, D.L. and Pilson, M.E.Q. 1972. Spectrometric determination of arsenite, arsenate and phosphate in natural waters. *Anal. Chim. Acta.* **58:** 289-299.

Keren, R.and Talpaz, H. 1984. Boron adsorption by montmorillonite as affected by particle size. *Soil Sci. Soc. Am. J.* **48**: 555–559.

Kuo, S. 1996. Phosphorus. In(J.M. Bartels, and J.M. Bigham Eds.) *Methods of Soil Analysis*,

Part 3. Chemical Methods. SSSA Book Series No. 5, pp. 869-920

Lin, Z., and Puls, R.W. 2000. Adsorption, desorption and oxidation of arsenic affected by clay minerals and aging processes. *Environ Geol.* **39:**753–759

Loeppert, R.H. and Inskeep, W.P. 1996. Iron. In(DL Sparks *et al.* Eds) *Methods of soil analysis*. Part 3. Chemical methods., Soil Science Society of America Inc, American Society of Agronomy Inc.: Madison, WI, U. S. A., pp. 648–651.

Majumdar, K. and Sanyal, S.K. 2003. pH-Dependent arsenic sorption in an Alfisol and an Entisols of West Bengal. *Agropedo.***13**: 25-29.

Mandal, B.K.and Suzuky, K.T. 2002. Arsenic round the world: a review. *Talanta***58**: 201–235.

Manning, B.and Goldberg, S. 1996. Modeling arsenate competitive adsorption on kaolinite, montmorillonite, and illite. *Clays and Clay Minerals* **44**: 609-623.

Masscheleyn, P.H., Delaune, R.D. and Patrick, W.H. 1991. Arsenic and selenium chemistry as affected by sediment redox potential and pH. *J. Environ. Qual.* **20**: 522-527.

Matera, V. and Le Hecho, L. 2001. Arsenic Behavior in Contaminated Soils: Mobility and Speciation. In(H.M. Selim and D.L. Sparks, Eds) Heavy Metals Release in Soil, Lewis Publisher, Boca Raton, pp 207–235.

McLaren, R.G., Naidu, R., Smith, J. and Tiller, K.G. 1998. Fractionation and distribution of arsenic in soils contaminated by cattle dip. *J. Environ. Qual.***27:** 348-354.

Mohapatra, D., Mishra, D., Roy Choudhury, G. and Das, R.P. 2007. Arsenic adsorption mechanism on clay minerals and its dependence on temperature. *Korean J. Chem. Eng.* **24**: 426–430.

Moreno-Jiménez, E., Esteban, E. and Peñalosa, J.M. 2012. The Fate of Arsenic in Soil-Plant Systems. In (D.M. Whitacre, Ed.) *Reviews of Environmental Contamination and Toxicology*, Springer, New York **215:** 1-37

Mortland, M.M. and Kemper, W.D. 1965. In (C.A. Black *et al.*, Eds.) *Methods of Soil Analysis*, part 2. Agron, Monogr. 9. Am. Soc. Agron, Madison, Wisconsin, U.S.A., pp. 532.

Muljadi, D., Posner, A.M. and Quirk, J.P. 1966, The mechanism of phosphate adsorption on kaolinite, gibbsite and pseudo-boehmite. I. The isotherms and the effect of pH on adsorption. *J Soil Sci.* **17**: 212–228.

Norra, S., Berner, Z.A., Agarwala, P., Wagner, F., Chandrasekharam, D. and Stuben, D. 2005. Impact of irrigation with As rich groundwater on soil and crops: a geochemical case

study in Maldah district, West Bengal. *Appl. Geochem.***20:**1890-1906.

Oscarson, D.W., Huang, P.M. and Liaw, W.K. 1980. The oxidation of arsenite by aquatic sediments. *J. Environ. Qual.* **9**: 700-703.

Sadiq, M.1997. Arsenic chemistry in soils: an overview of thermodynamic predictions and field observations. *Water Air Soil Pollut.* **93:** 117–136.

Sanyal, S.K., Gupta, S.K., Kukal, S.S. and Jeevanrao, K. 2015. Soil Degradation, Pollution and Amelioration. In(H. Pathak, S.K. Sanyal and P.N. Takkar Eds.) *State of Indian Agriculture-Soil*, National Academy of Agricultural Sciences, New Delhi, pp. 234-266.

Sanyal, S.K., Poonia, S.R. and Baruah, T.C. 2009. Soil Colloid s and Ion Exchange in Soil. In (N.N. Goswami *et al.* Eds.) *Fundamentals of Soil Science*, Second Edition, Indian Soc. SoilSci.,New Delhi, pp. 269-315.

Sanyal, S.K. 2005. Arsenic contamination in agriculture: A threat to water-soil-crop-animal-human continuum. Presidential Address, Section of Agriculture & Forestry Sciences, 92nd Session of the Indian Science Congress Association (ISCA), Ahmedabad, January 3-7, 2005; The Indian Science Congress Association, Kolkata.

Sanyal,S.K., Jeevanrao, K. and Sadana, Upkar S. 2012.Toxic Elements and Other Pollutants-A Threat to Nutritional Quality. In (N. N. Goswami *et al.*, Eds.) *Soil Science in the Service of Nation*, Indian Soc. Soil Sci., New Delhi, pp. 266-291.

Saunders, W.M.H. 1965. Phosphate retention by New Zealand soils and its relationship to free sesquioxides, organic matter and other soil properties. *New Zeal. J. Agric. Res.* **8:** 30-57.

Smedley, P.L. and Kinniburgh, D.G. 2002. A review of the source, behaviour and distribution of arsenic in natural waters. *Appl Geochem.* **17**: 517–568.

Sparks, D.L., Page, A.L., Helmke, P.A., Loeppert, R.H., Soltanpour, P.N., Tabatabai, M.A., Johnston, C.T. and Sumner, M.E. 1996. In (D.L. Sparks *et al.*, Eds.) *Methods of Soil Analysis.* Part 3. Chemical Methods, Soil Science Society of America Inc., American Society of Agronomy Inc.: Madison, WI, U. S. A.

Sumner, M.E. and Miller, W.P, 1996. Cation exchange capacity and exchange coefficients. In (D.L. Sparks *et al.*, Eds.) *Methods of Soil Analysis.* Part 3. Chemical Methods, Soil Science Society of America Inc., American Society of Agronomy Inc.: Madison, WI, U. S. A., pp. 1218–1220.

Sun, X. and Doner, H.E. 1998. Adsorption and oxidation of arsenite on goethite. *Soil Sci.* **163:** 278-287.

Swartzen-Allen, L.S. and Matijevic, E. 1974. Surface and colloid chemistry of clays. *Chem. Rev.* **74**: 385–400.

Tu,C., Ma, L.Q., Zhang,W.,Cai, Y., Harris, W.G. 2003. Arsenic Species and leachability in the fronds of the hyperaccumulator Chinese brake (*Pteris vittata* L.). *Environ. Pollut.* **124:** 223-230.

Vela, N.P., Heitkemper, D.T. and Stewart, R.K. 2001. Arsenic extraction and speciation in carrots using accelerated solvent extraction, liquid chromatography and plasma mass spectrometry. *Analyst.***126:** 1011-1017.

Violante, A., Gaudio, S.D., Pigna, M., Pucci, M.and Amalfitano, C. 2008. Sorption and Desorption of Arsenic by Soil Minerals and Soils in the Presence of Nutrients and Organics. In(Q. Huang., P.M. Huang. and A. Violante. Eds) *Soil Mineral Microbe-Organic Interactions,* Springer, pp. 39-69.

Woolson, E.A. 1977. Generation of alkylarsines from soil. *Weed Sci.* **25**: 412-416.

Zhang, H. and Selim, H.M. 2008. Reaction and transport of arsenic in soils: equilibrium and kinetic modelling. *Adv. Agron.* **98**: 45–115.

Zhao, F.J., Ma, F., Meharg, A.A. and McGrath, S.P. 2009. Arsenic uptake and metabolism in plants. *New Phytol.* **181** : 777–794.

(Received June 2016; Accepted September 2016)

Clay Research, Vol. 34, No. 2, pp. 80-90 (2015)

Preparation and Characterization of Nanoclay Polymer Composites (NCPCs) Loaded with Urea

KIRTI SAURABH, K.M. MANJAIAH*, S.C. DATTA AND RAJESH KUMAR**

Division of Soil Science and Agricultural Chemistry, ICAR- Indian Agricultural Research Institute, New Delhi 110012
***Division of Agricultural Chemicals, ICAR- Indian Agricultural Research Institute, New Delhi 110012*

Abstract–*In the present paper, three slow release clay-polymer nanocomposite fertilizers were synthesized, (1) acrylic acid + acrylamide (AA +Am NCPC) (2) acrylic acid + wheat flour starch (WF NCPC) and (3) acrylic acid + sodium alginate (Na-Alg NCPC) via free radical polymerization in the presence of bentonite. The nanocomposites were characterized by XRD, FTIR, SEM and SEM-EDX. Results revealed that NCPCs were participated in the graft polymerization reaction with AA and the bentonite layers were exfoliated and basically dispersed in the composites on a nanoscale after the polymerization. The three (AA +Am, WF and Na-Alg) polymer nanocomposite synthesized under optimum reaction conditions exhibits the maximum swelling ratio of 68.5, 54.3, and 81.9 g/g in distilled water respectively. The nitrogen analysis of WF, AA+AM and Na-Alg NCPC was 19.10, 24.13% and 26.07%, respectively. The N release percentage at 30th day in soil reached around 87.22, 59.91, 63.77 and 60% of total applied N for Urea, AA+AM, WF and Na-Alg NCPC, respectively. In this way NCPCs showed the double function that delays nitrogen release and stores water in it.*

Key words: Nanoclay polymer composite, FTIR, SEM-EDX, XRD, water absorption, Urea

Most of the hydrogels are made from synthetic hydrophilic, petroleum-based polymers such as poly (acrylic acid) or its copolymer with poly (acrylamide) whereas the demand for using natural hydrogels such as starch, cellulose, chitosan, and alginate (Rashidzadeh & Olad, 2014) as fertilizer carriers, due to their biodegradability and low costs, is continuously increasing. Biopolymers like starch and alginate, being a renewable and eco-friendly biodegradable materials are gaining considerable importance in agriculture to be used as a fertilizer carrier (Jin *et al*., 2013). Though these polymers have great significance as slow release fertilizer carrier, the high cost of such products in the market ends up making its application impractical. Therefore, to enhance the fertilizer performance and to reduce the cost, many researchers had used naturally available inorganic clays such as montmorillonite and hectorite, rectorite, attapulgite, kaolin, clinoptilolite (Rashidzadeh *et al*., 2014) in high proportions in polymer composites. Moreover, it has been proved that the inclusion of inorganic clays into hydrogels decreases the release rate of fertilizer from a slow release formulation (Liang and Liu, 2006; Liang *et al.,* 2007). Therefore, in the present work, attempt was done to prepare three different types of fertilizer polymer nanocomposites and evaluated the swelling behavior and slow release fertilizer properties.

Material and Methods

Synthesis of nanoclay-polymer composites (NCPCs)

Acrylic acid (AA) + acrylamide (Am) NCPCs

***Corresponding Author Email :** manjaiah@iari.res.in

and sodium alginate (Na-Alg) NCPCs were synthesized from commercially available nano bentonite through the process as described by Liang and Liu, (2007) and Shi *et al.*, (2012), respectively with some modifications. For starch based nanocomposite a 10 g of wheat flour powder and 30 ml of distilled water was put in a 250-m four-necked ask equipped with a stirrer, a condenser, a thermometer and a nitrogen line. The slurry was heated to 80 ^{0}C for 30 min under nitrogen atmosphere in the presence of initiator ammonium persulphate (APS) (0.32 g). After 15 min, 10 ml of AA with 60% neutralization degree (neutralized ammonia) and crosslinker N,Ñ-methylene bisacryamide (MBA) (0.13 g) and bentonite clay of 10% weight of AA was added. Then the temperature was increased gradually to 70 ^{o}C in presence of nitrogen gas and kept for 1 h. The resulting product was then dried at 70 ^{0}C to a constant weight and milled.

The loading of urea carried out by immersing pre-weighed dry gels into the aqueous solution of these compounds for 20 h to reach swelling equilibrium. Thereafter, the swollen gels were dried at 60^{o}C for 6 days. Finally the dried products were milled and screened. Nitrogen content in the sample was analyzed by Kjeldhal digestion method and the N content in AA +Am NCPC, WF NCPC and Na-Alg NCPC was 24.13%, 19.1% and 26.07%, respectively.

A weighted quantity of nanocomposite (1 g) was immersed in distilled water (500 ml) at room temperature to reach the swelling equilibrium. Swollen samples were then separated (at time interval of 2, 4, 8,1,16, 20, 24, and 30 hours) from unabsorbed water by ltering over a 100-mesh screen. The water absorbency composite was determined by weighing the swelled samples (Mo *et al.*, 2006).

Nitrogen release behavior of NCPCs in soil was studied, by conducting a laboratory incubation experiment in which NCPCs (to give 200 mg N kg^{-1} soil) were well mixed with 50 g of dry soil (< 2 mm) kept in a 150 ml glass beaker covered and incubated for dierent periods at room temperature. Soil samples (10 g) from the incubated soils (destructive samples) were drawn after 7, 14, 21, and 30 days of incubation and NH_4^+ and NO_3^- - N were estimated by following the method given by Keeney and Nelson (1982). The statistical design followed a completely randomized design (CRD) with three replicates.

Characterization of NCPCs

The characteristic functional groups of the bentonite, polymer, urea, and NCPCs were analyzed by Fourier transform infrared spectrometry (FTIR) in the region of 4000 - 600 cm^{-1} using KBr pellets. Wide angle X-ray diffraction patterns of NCPCs and bentonite were recorded using a Philips PW1710 X-ray diffractometer employing Cu-Kα radiation with a Ni lter. The tube current was 20 mA with a tube voltage of 40 kV. The 2θ angular regions between 3 and 50^o were explored. Scanning electron microscopy (SEM) studies was done with Zeiss EVOMA10, to observe the surface morphological aspects of the prepared NCPCs and also the clay minerals. The energy dispersive X-ray (EDX) analysis was simultaneously carried out to know the elemental composition of those samples.

Results and Discussion

Infrared spectroscopy (FTIR)

The FTIR spectra of (a) Urea, (b) Bentonite, (c) Wheat flour (WF) powder, (d) Na-Alg powder, (e) AA+Am NCPC, (f) WF NCPC and (g) Na-Alg NCPC are shown in figure 1. The characteristic peaks at 1032 cm^{-1} due to the Si-O stretching, and 912, 3619, and 3442 cm^{-1} due to the -OH group were found in the commercial bentonite (Figure 1b). After the formation of nanocomposites the two absorption peaks (912, 3619 cm^{-1}) of -OH group of bentonite disappeared due to polymerization (Figure 1b,e,f and g).

Disappearance of peaks after polymerization confirmed that phenomena of graft copolymerization between -OH groups on bentonite and monomers took place. Santiago *et al.*, (2006) also reported the similar conclusion that hydroxyl groups on the surface of bentonite would react with the carboxyl group of poly (SA) and sodium bentonite particles could be acted as cross-link points developed some sort of bonding with the polymer.

The FTIR spectrum of the urea (Figure 1a)

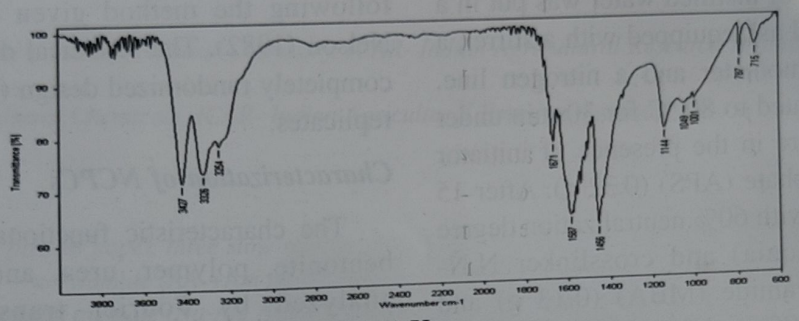

(a) Urea

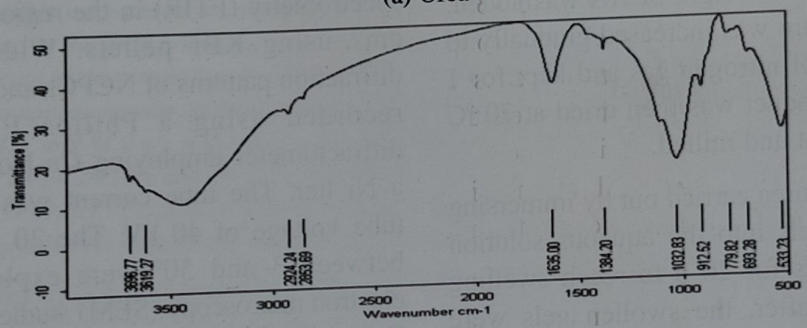

(b) Bentonite

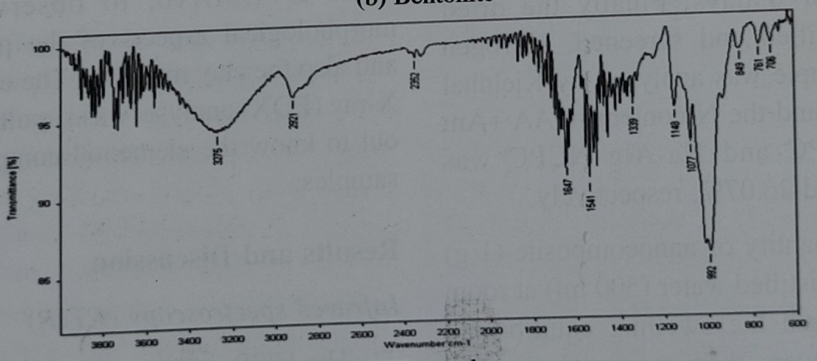

(c) WF powder

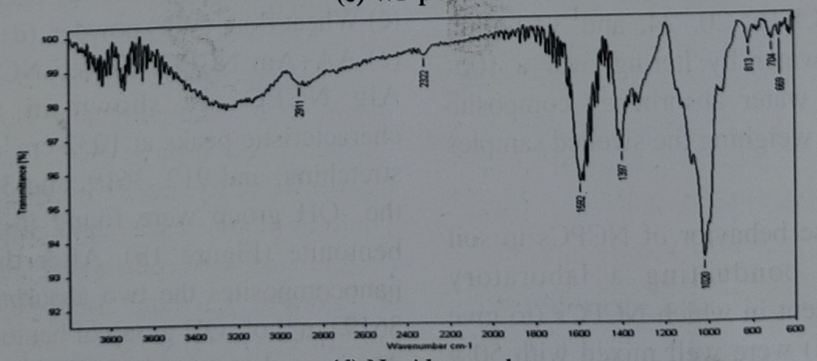

(d) Na-Alg powder

showed the characteristic carbonyl peak at 1671 cm^{-1} (C=O), and two N-H absorbency bands at 3427 and 3326 cm^{-1}. In the IR spectrum of NaAlg (Figure 1d), the broad peak which was present between 3000-3400 cm^{-1} is characterized as the H-bonded O–H stretching frequency. The band at approximately 2911 cm^{-1} is assigned to C–H stretching. Although the fingerprint region (1000 – 750 cm^{-1}) is seldom looked into in detail by researchers, it is the most discussed region in carbohydrates. The peaks at 1300, 1020 and 947 cm^{-1} are all due to stretching vibrations of C–O from glycosidic bonds, with the stretching vibration of C–O–C from glycosidic bonds contributes to the peak at 947 cm^{-1} as well. In addition, there are two peaks at 1592 and 1397 cm^{-1} indicating the COO^{-} stretching group attached to the sodium ion. The former is caused by the asymmetric stretching vibration of the carboxylate COO^{-} while the latter is deduced to be due to C–OH deformation vibration with contribution of COO^{-} symmetric stretching vibration of the carboxylate group.

The characteristic absorption band of NaAlg (Figure 1d) at 1020 cm^{-1} (stretching vibration of C–OH groups) were obviously weakened after reaction, which indicate the –OH groups of NaAlg participate in chemical reaction. In FT-IR spectra of Na-Alg NCPC (Figure 1g), the bands at 1683 cm^{-1} is related to the stretching vibration of the carbonyl groups of AA. The bands in Na-Alg NCPC at 1594 and 1457–1410 cm^{-1} were assigned to the asymmetric and symmetric stretching vibration of the $-COO^{-}$ groups, respectively (Shi *et al.*, 2012). It was observed that the absorption bands of carbonyl at 1673 cm^{-1} in both AA+Am NCPC and WF NCPC and at 1683 cm^{-1} in Na-Alg NCPC might be due to the formation of hydrogen bonding between the carboxyl and carbonyl groups of the hydrogel materials and the hydroxyl groups of Al-OH and Si-OH in bentonite (Hua & Wang, 2009).

According to Jin *et al.*, (2013) the infrared spectrum of starch showed a characteristic absorption band at 3275–3655 cm^{-1} (Figure 1c), which corresponded to the stretching vibration of O-H (carbons 2, 3, and 6). The band was wide and gentle because of free and associated hydroxyl groups generated by hydrogen bonding. Copolymerization brought the carboxylic groups into the polymer, which increased the intramolecular and intermolecular hydrogen bonding, so the band became sharper, and there was a shift from 3275 to 3253 cm^{-1} (Figure 1f), which was due to the formation of intermolecular hydrogen bonding between starch and poly (AA) and a negative shift from 3655 to about 3429 cm^{-1} due to the decrease in content of free hydroxyl groups, as shown in Figure 1f. The peak observed at 2921 cm^{-1} (Figure 1(A)WF) corresponded to the stretching vibration of saturated C–H groups, which shifted from 2921 to 28972 cm^{-1} (Figure 1(B)) due to the addition of grafting polymer chains. The characteristics for the saccharide structure of starch were appearing at 1647 and 1148 cm^{-1}, as shown in Figure 1c, which could be assigned to symmetric and asymmetric stretching vibrations of the C–O–C bridge, respectively. It was evident that a stronger and wider peak appearing at about 1673 cm^{-1}, shown in Figure 1f, was due to the symmetric stretching vibration of the C–O–C bridge. The peak of bentonite at 1032.83 cm^{-1}, due to Si-O group, is also observed with slight shift to 1062 cm^{-1} in Na-Alg NCPC, whereas very weak peak was observed in both AA+Am and WF NCPCs indicates the incorporation of the bentonite into the superabsorbent.

X-ray diffraction analysis

The XRD was used to confirm the mineralogy of the bentonite clay and polymerization of NCPCs. XRD patterns of the commercial bentonite clay confirmed the presence of montmorillonite as a major phase because, the peak at 2θ=6.8 (d spacing =13.01 ´) corresponds to smectite (2:1 mineral) (Figure 2a). The XRD pattern of AA+Am NCPC, WF NCPC and Na-Alg NCPC did not show the characteristic basal

peak of bentonite particles after their incorporation into the polymer matrix (Figure 2c, d and e). This indicates that the silicate layers of bentonite were completely exfoliated in final product after polymerization process. According to Leitão *et al.*, (2015), clay particles dispersed in the nanocomposite matrix due the formation of H-bonds between the amide and acid groups present on the polymer matrix and water molecules surrounding the exchangeable cations on clay particles. The exfoliated nature of the nanoclay was due to the long polymer chains of the polymer matrix that were inserted into the gallery space of the nanoclay, leading to an

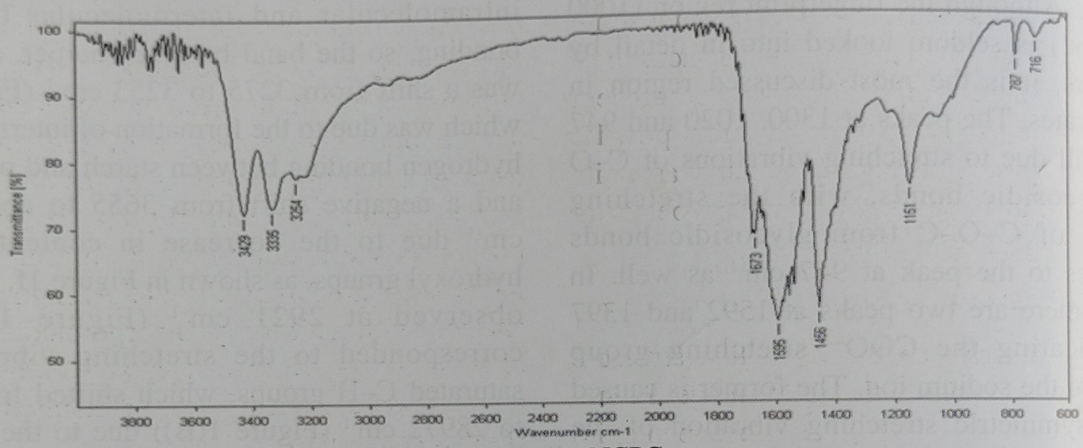

(e) AA+Am NCPC

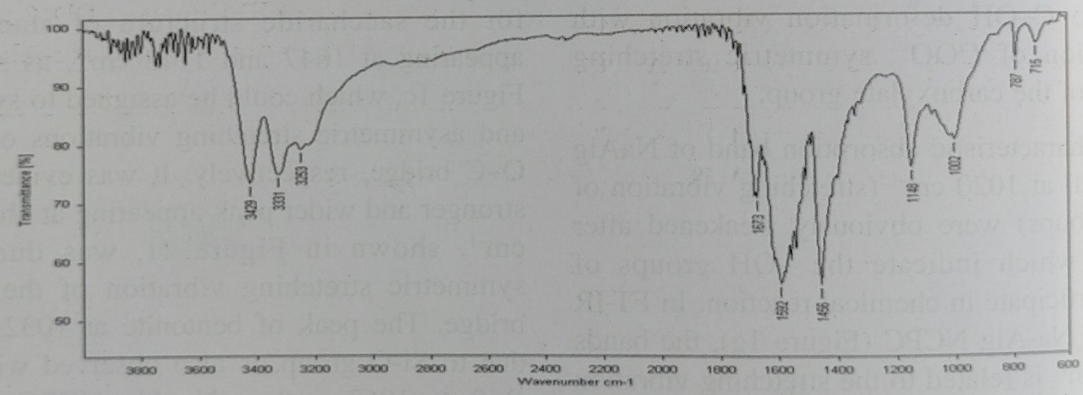

(f) WF NCPC

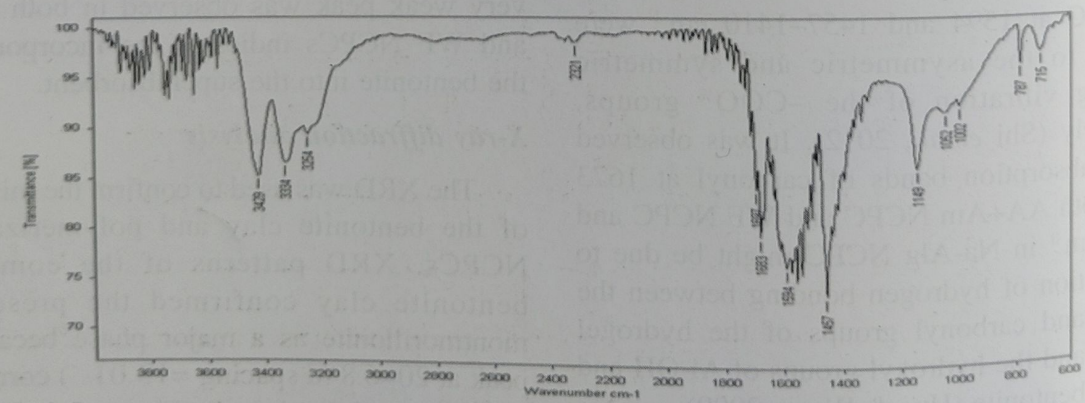

(g) Na-Alg NCPC

Fig. 1. *FTIR spectra of (a) Urea, (b) Bentonite, (c) WF powder, (d) Na-Alg powder, (e) AA+Am NCPC, (f) WF NCPC and (g) Na-Alg NCPC*

increase in the interlayer spacing of the silicate layers. The extensive layer separation associated with exfoliated structures disrupts the coherent layer stacking and results in a featureless diffraction pattern. Thus, the reason for the no diffraction peaks of exfoliated structures in XRD diffractograms are either because of a very large spacing between the layers (i.e. exceeding 8 nm in the case of an ordered exfoliated structure) or because the nanocomposite does not present ordering. The XRD spectra of urea powder showed its crystalline nature which was quite clear from the occurrence of sharp peaks at specific Bragg's angles (Figure 2f).

Scanning electron microscopy (SEM)

We can clearly see the plate like structure exhibited by bentonite in the SEM image (Figure 3a). Masindi *et al.*, (2015) described bentonite clay as leafy, lamella like structures with several pores. SEM micrograph of WF NCPC showed highly porous and honeycomb like structure with highly dispersed clay particles as compared to AA+Am and Na-Alg NCPCs (Figure 3b,c & d). Further it could be seen that the surface of NCPCs made with sodium alginate was having more number of pores with open channel than others (Figure 3d). Rashidzadeh & Olad, (2014) found higher absorption of water by NaAlg-g-poly (AA-co-Am)/ montmorillonite encapsulated NPK fertilizer, as montmorillonite act as the physical crosslinking agent, therefore homogeneity as well as the pore size structure of the copolymer decreases, but the number of pores and channels increases and, consequently, the hydrogel with clay was expected to swell more. AA+Am NCPCs (Figure 3b) displayed the rough and loose surface with uniformly incorporated bentonite clay in the polymer matrix and enhanced the water uptake capacity of the nanocomposites (Leitao *et al.* 2015).

In addition to SEM images, EDX spectra of the bentonite, AA+Am, WF and Na-Alg NCPCs

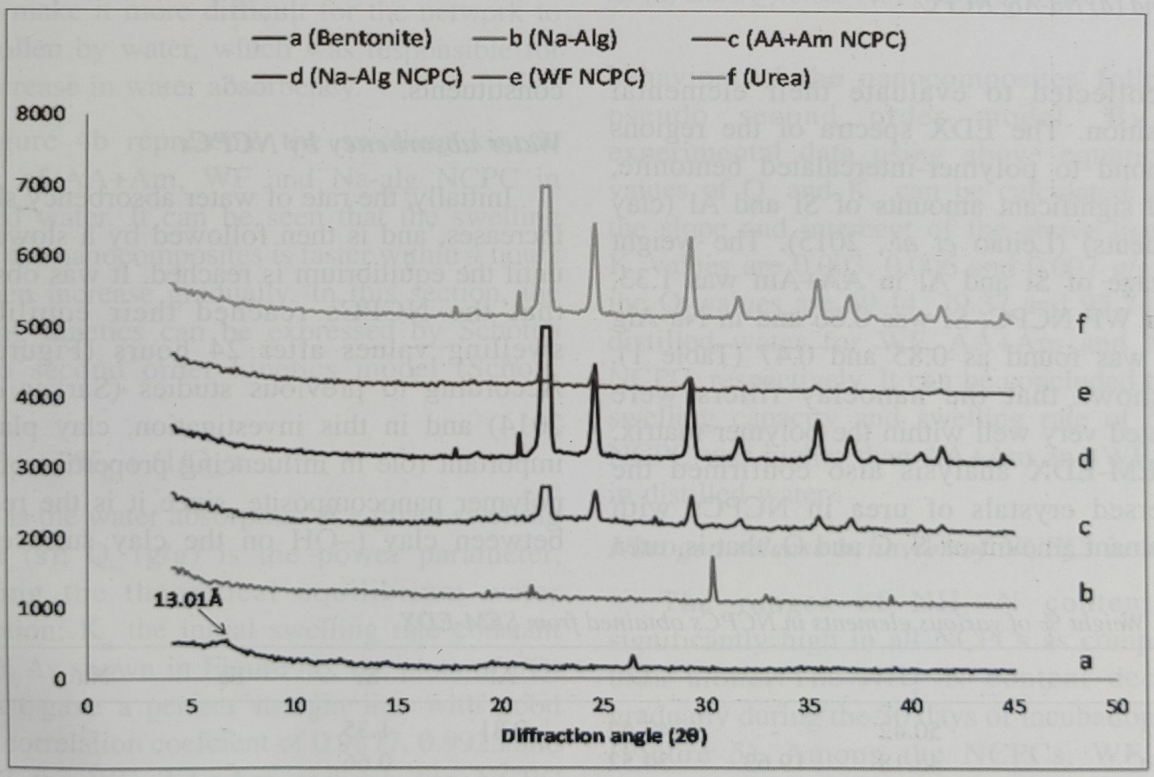

Fig. 2. *Random oriented powder XRD patterns of (a) bentonite, (b) Na-Alg powder (c) AA+Am NCPC, (d) Na-Alg NCPC, (e) WF NCPC and (f) Urea*

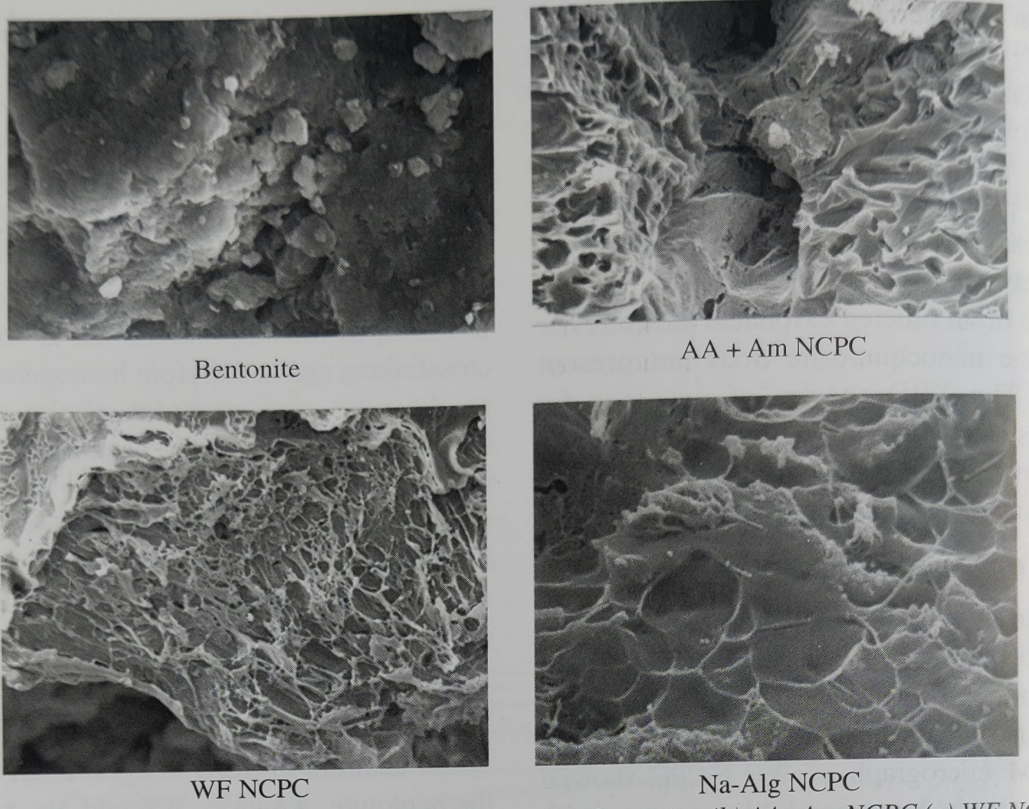

Fig. 3. *Scanning electron microscopy (SEM) images of (a) bentonite, (b) AA+Am NCPC (c) WF NCPC and (d) Na-Alg NCPC*

were collected to evaluate their elemental composition. The EDX spectra of the regions correspond to polymer-intercalated bentonite, showed significant amounts of Si and Al (clay constituents) (Leitão *et al.*, 2015). The weight percentage of Si and Al in AA+Am was 1.33, 0.66, in WF NCPC, Si was 0.66 and in Na-Alg NCPC was found as 0.85 and 0.47 (Table 1). That shows that the nanoclay fillers were distributed very well within the polymer matrix. The SEM-EDX analysis also confirmed the redispersed crystals of urea in NCPCs with predominant amount of N, C and O, that is, urea constituents.

Water absorbency by NCPCs

Initially, the rate of water absorbency sharply increases, and is then followed by a slower rate until the equilibrium is reached. It was observed that the NCPCs reached their equilibrium swelling values after 24 hours (Figure 4a). According to previous studies (Sarkar *et al.*, 2014) and in this investigation, clay plays an important role in influencing properties of clay-polymer nanocomposite, since it is the reaction between clay (–OH on the clay surface) and

Table 1. *Weight % of various elements in NCPCs obtained from SEM-EDX*

	C	N	O	Al	Si	Fe	Na	Total
Bentonite	50.42	-	47.42	0.81	1.35	-	-	100
WF NCPC	45.18	19.63	34.52	-	0.66	-	-	100
AA+AM NCPC	46.63	22.16	28.12	0.66	1.33	1.10	-	100
Na-Alg NCPC	43.06	25.73	28.79	0.47	0.85	-	1.10	100

monomers that form composite polymeric network results in increased water absorption. The equilibrium water absorbance by the AA+Am, WF and Na-Alg NCPC were 68.5, 54.3 and 81.9 g/g, respectively (Figure 4a). Dense polymeric network and more number of large pores in AA+Am and Na-Alg NCPC resulted in more water absorption by them as compared to WF NCPC. Whereas, smaller three-dimensional net hole due to the rather compact structure of the NCPC with 50 wt % starch resulted in less water absorption (Jin *et al.,* 2013). Rashidzadeh *et al.*, (2014) reported that due to negative surface charge of the clay, high repulsive forces between $-COO^-$ groups of polymer and negative surface charge of bentonite resulted in increased expansion of the hydrogel network and a higher swelling ratio. They also observed that, when clinoptilolite content was higher than 10 %, a further increase in the crosslinking density of the hydrogel network would decrease the space among the grids of the hydrogel network. This would make it more difficult for the network to be swollen by water, which was responsible for the decrease in water absorbency.

Figure 4b represents the swelling kinetic curves of AA+Am, WF and Na-alg NCPC in distilled water. It can be seen that the swelling rate of the nanocomposites is faster within 4 hours and then increase gradually. In this section, the swelling kinetics can be expressed by Schott's pseudo second order kinetics model (Schott, 1992).

$$t/Q_t = 1/K_{is} + (1/Q_\infty)t$$

Q_t is the water absorption at a given swelling time t (s); Q_∞ (g/g) is the power parameter, denoting the theoretical equilibrium water absorption; K_{is} the initial swelling rate constant (g/g s). As shown in Figure 4b, the plots of t/Qt versus t gave a perfect straight line with good linear correlation coefcient of 0.9877, 0.9925 and 0.9937 for WF, AA+Am and Na-Alg NCPC respectively, which indicates that the swelling

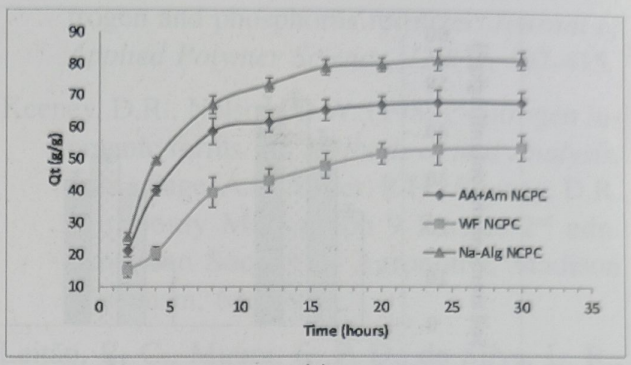

(a)

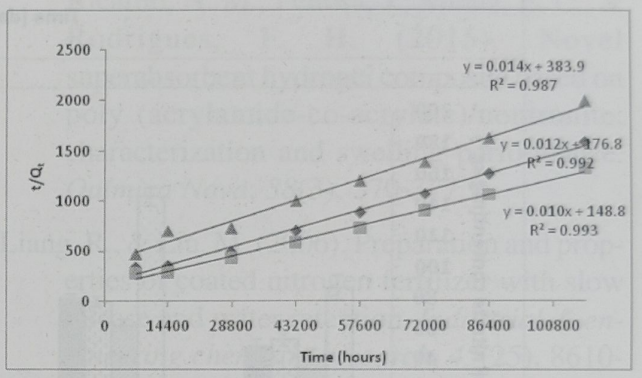

(b)

Fig. 4. *Swelling kinetic curves of NCPCs in distilled water (a) and t/Q_t versus t (b) graphs of NCPCs*

behaviors of the nanocomposites follow the pseudo second order model. By tting experimental data using above equation, the values of Q_∞ and K_{is} can be calculated through the slope and intercept of the above lines. The K_{is} values are 0.003, 0.006 and 0.007 g/g s, and the Q_∞ values are 69.44, 79.37 and 95.24 g/g in distilled water for WF, AA+Am and Na-Alg NCPC, respectively. It can be concluded that the swelling capacity and swelling rate of Na-Alg NCPC was higher than AA+Am and WF NCPC in distilled water.

Nitrogen release behavior of NCPCs in soil

The ranges of NH_4^+-N content were significantly high in all NCPCs as compared to urea alone. The NH_4^+-N content decreased gradually during the 30 days of incubation period (Figure 5). Among the NCPCs, WF NCPC showed higher NH_4^+-N concentration during the initial period of incubation which was 46.64,

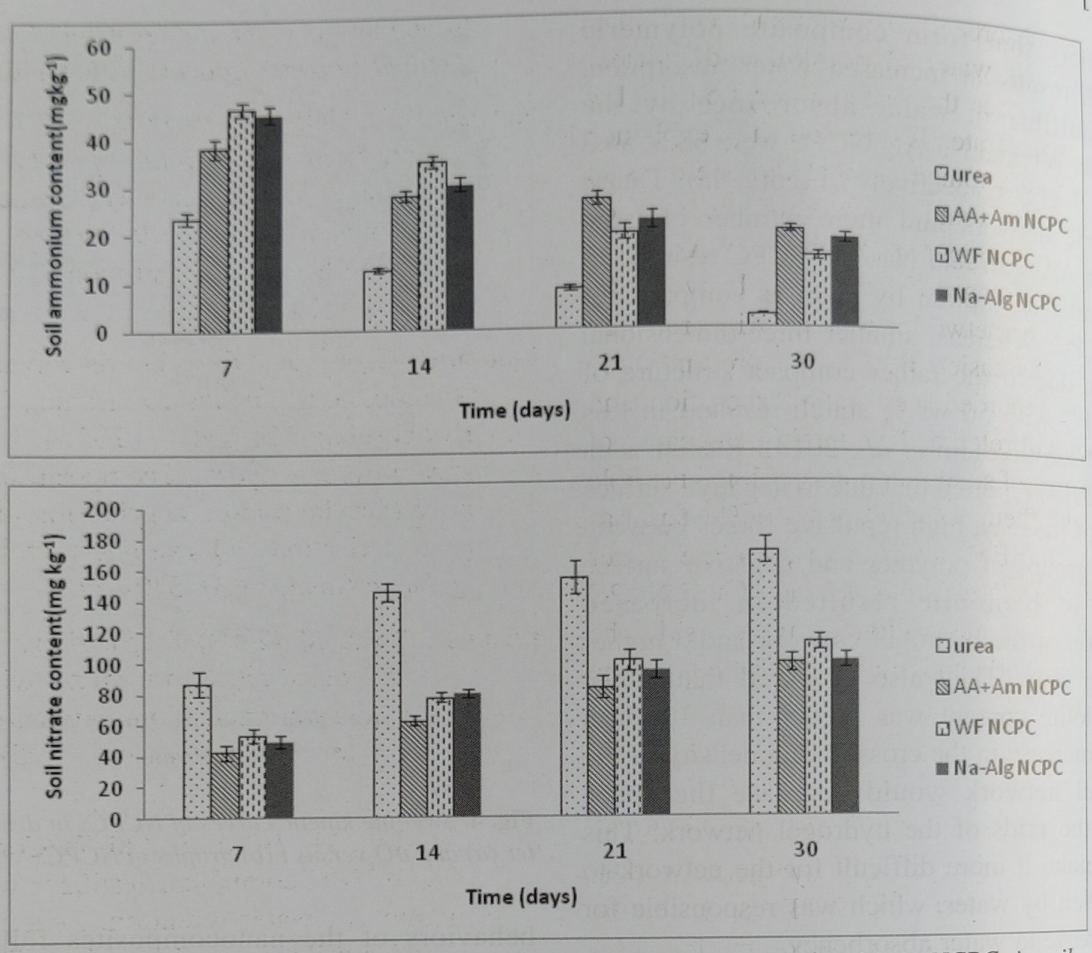

Fig. 5. *Release behavior of (a) NH_4^+ mg kg^{-1} soil and (b) NO_3^- mg kg^{-1} soil from NCPCs in soil*

34.82 mg kg^{-1} at 7 and 14th day whereas, its concentration decreased from 14th day onward and it was observed that 19.75 and 14.84 mg kg^{-1} of soil at 21 and 30th day of incubation, respectively. Less NO_3^--N content was observed in all the NCPC treatments compared to urea. The NO_3^--N content for WF NCPC was 53.9, 77.8, 101.3 and 112.7 mg kg^{-1} soil, for Na-Alg NCPC 49.9, 80.2, 94.7 and 101.3 7 mg kg^{-1} soil, and for AA+Am NCPC 43, 62.6, 83.7 and 99.47 mg kg^{-1} soil at 7, 14, 21 and 30th day of incubation, respectively. At the end of 30 day incubation, the percentage of mineral N (NH_4+NO_3) out of total applied N (200 mg kg^{-1} soil) were found in this order: urea (87.22%) > WF NCPC (63.78%)> Na-Alg NCPC (60%) > AA+Am NCPC (59.91%) (Figure.6). The slow release property of these NCPCs resulted in the higher accumulation of the ammonium ions which leads to their slow conversion into the nitrate nitrogen by the microbes in soil.

Jin *et al.,* (2013) reported in their study that

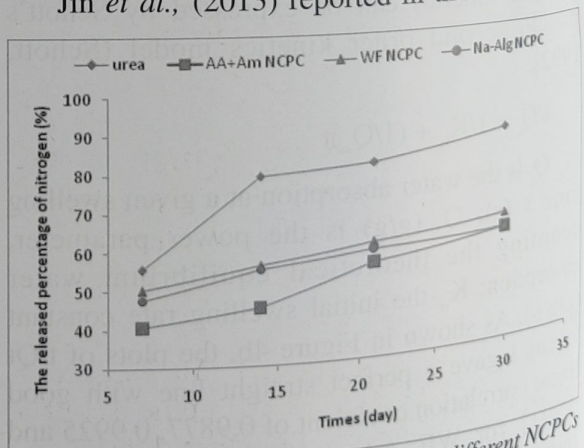

Fig. 6. *Nitrogen release behaviour from different NCPCs in soil*

starch superabsorbent fertilizers showed similar trend for both water absorption and nutrient release i.e. higher the water absorption, higher was the release rate. The reason they explained behind such phenomena is that the apertures in the three-dimensional network of the swollen hydrogel were bigger with higher WAs. As a result, the exchange of free water between the solution and the network and the nutrient released through it was easier. But, in the present study WF NCPC recorded less water absorption and higher nutrient release. This might be because of larger number of small three-dimensional net hole which make them compact at 50 wt% starch as observed in SEM micrograph, so the water absorption was less. Less swelling of WF NCPC resulted in less absorption of urea inside the hydrogel network and more adsorption on the surface of NCPC.

Conclusions

Three different types of slow release fertilizers were successfully synthesized. The FTIR, SEM, SEM-EDX, and XRD confirmed the incorporation of bentonite with polymeric matrix in different NCPCs and occurrence of graft polymerization. The Schott's pseudo second order kinetics model presented the order of maximum water absorbency by different NCPCs. The nitrogen release rate was close to 65% on the 30th day from the NCPCs there by signifying their potential use as slow release products.

References

Hua, S. and Wang, A. (2009). Synthesis, characterization and swelling behaviors of sodium alginate-g-poly (acrylic acid)/sodium humate superabsorbent. *Carbohydrate Polymers*, *75*(1), 79-84.

Jin, S., Wang, Y., He, J., Yang, Y., Yu, X., & Yue, G. (2013). Preparation and properties of a degradable interpenetrating polymer networks based on starch with water retention, amelioration of soil, and slow release of nitrogen and phosphorus fertilizer. *Journal of Applied Polymer Science*, *128*(1), 407-415.

Keeney, D.R., Nelson, D.W. (1982): Nitrogen inorganic forms. In: *Methods of Soil Analysis.* (eds.) Page, A.L, Miller, R.H., Keeney, D.R. Agronomy Monograph 9 Part 2, 2nd edn. American Society of Agronomy, Madison Wisconsin, 643-698.

Leitão, R. C., Moura, C. P. D., da Silva, L. R., Ricardo, N. M., Feitosa, J., Muniz, E. C., & Rodrigues, F. H. (2015). Novel superabsorbent hydrogel composite based on poly (acrylamide-co-acrylate)/nontronite: characterization and swelling performance. *Química Nova*, *38*(3), 370-377.

Liang, R., & Liu, M. (2006). Preparation and properties of coated nitrogen fertilizer with slow release and water retention. *Industrial & engineering chemistry research*, *45*(25), 8610-8616.

Liang, R., Liu, M., & Wu, L. (2007). Controlled release NPK compound fertilizer with the function of water retention. *Reactive and Functional Polymers*, *67*(9), 769-779.

Masindi, V., Gitari, M. W., Tutu, H., & DeBeer, M. (2015). Efficiency of ball milled South African bentonite clay for remediation of acid mine drainage. *Journal of Water Process Engineering*, *8*, 227-240.

Mo, C., Shuquan, Z., HuaMin, L., Zhanbin, H., Shuqin, L. (2006). Synthesis of poly (acrylic acid)/sodium humate superabsorbent composite for agricultural use. *Journal of Applied Polymer Science,* 102(6): 5137-5143.

Ni, B., Liu, M., Lu˜, S., Xie, L., Zhang, X., & Wang, Y. (2010). Novel slow-release multielement compound fertilizer with hydroscopicity and moisture preservation. *Industrial & Engineering Chemistry Research*, *49*(10), 4546-4552.

Rashidzadeh, A., & Olad, A. (2014). Slow-released NPK fertilizer encapsulated by NaAlg-g-poly

(AA-co-AAm)/MMT superabsorbent nanocomposite. *Carbohydrate polymers*, *114*, 269-278.

Rashidzadeh, A., Olad, A., Salari, D., & Reyhanitabar, A. (2014). On the preparation and swelling properties of hydrogel nanocomposite based on Sodium alginate-g-Poly (acrylic acid-co-acrylamide)/ Clinoptilolite and its application as slow release fertilizer. *Journal of Polymer Research*, *21*(2), 1-15.

Santiago, F., Mucientes, A. E., Osorio, M., & Poblete, F. J. (2006). Synthesis and swelling behaviour of poly (sodium acrylate)/sepiolite superabsorbent composites and nanocomposites. *Polymer international*, 55(8), 843-848.

Sarkar, S., Datta, S. C., & Biswas, D. R. (2014). Synthesis and characterization of nanoclay–polymer composites from soil clay with respect to their waterholding capacities and nutrientrelease behavior. *Journal of Applied Polymer Science*, 131(6).

Schott, H. (1992). Swelling kinetics of polymers. *Journal of Macromolecular Science B*, 31, 1–9.

Shi, X., Wang, W., Kang, Y. and Wang, A. (2012). Enhanced swelling properties of a novel sodium alginatebased super absorbent composites: Na Alggpoly (NaAcoSt)/APT. *Journal of Applied Polymer Science*, *125*(3), 1822-1832.

(Received April 2016; Accepted June 2016)

Clay Research, Vol. 34, No. 2, pp. 91-98 (2015)

Weathering of Silicate Minerals by Humic Acids : IV. Change in Surface Characteristics

SRUTI DAS, KUNAL GHOSH AND CHANDRIKA VARADACHARI

Raman Centre for Applied and Interdisciplinary Sciences, 16A Jheel Road, Kolkata 700 075

Abstract–*This study investigated the alterations of surfaces of primary silicate minerals after reaction with humic acid (HA). The silicates studied were olivine, epidote, tourmaline, hornblende, biotite and microcline; HA was extracted from an Alfisol. The weathered residues were studied with petrographic microscope and scanning electron microscope (SEM). Petrographic microscopy revealed the deposition of HA on the mineral surface. This deposition appeared to be highest with tourmaline followed by olivine, epidote and then hornblende, microcline and finally least with biotite. SE micrographs showed etching and pitting of the surface of almost all the minerals, including tourmaline and microcline. There was deposition of fine material on the surfaces of epidote, hornblende and biotite. Deposition of humic material on mineral surfaces reaffirms the dissolution-precipation mechanism proposed earlier from kinetic studies. Only biotite remained almost intact with slight fraying of edges. It appears that in contrast to weathering by water or small molecular weight organic acids, weathering by humic acid does cause signifcant degradation of tourmaline and microcline.*

Key words *:* Humic acids, petrographic microscopy, scanning electron microscopy, silicates, weathering.

A series of studies have been conducted on the weathering of primary silicates by humic acids (Das *et al*., 2013, 2014a, 2014b). These studies focussed on the nature of cation dissolution and residual products from weathering of six different silicates by humic acids (HAs) of diverse origin. These studies provide an understanding of the differences in reactivity amongst the silicate series, from the ortho to the tecto silicate and shows how crystal structure influencs the dissolution of cations from silicates. Both olivine and tourmaline showed reduction in $Fe^{2+/3+}$ with drastic changes in the XRD patterns of olivine; even tourmaline showed significant reduction in its strongest XRD peak (Das *et al*., 2013). Biotite was minimally altered whereas hornblende had significant loss of $Fe^{2+/3+}$ and Ca^{2+} and disappearence of its major XRD bands (Das *et al*., 2014a). Microcline showed great stability to HAs and minimal alteration of its XRD peaks; on the contrary, epidote was significantly altered with loss of Si^{4+}, $Fe^{2+/3+}$ and Ca^{2+} and alterations of XRD peaks (Das *et al*., 2014b). The common feature of all minerals was that they dissolved incongruently in HAs and dissolution followed a pattern of crests and troughs signifying intervals of dissolution and precipitation (Das *et al*., 2013, 2014a, 2014b). All studies suggested surface alterations and deposition of altered phases.

Earlier Barman *et al*. (1992) studied silicate dissolution by organic acids and showed that relative solubilities of the cations from a mineral depend on their positions within the crystal as well as the crystal structure. Silicates did not show any unique stability sequence. Dissolution occured by formation of a ligand-cation complex at the surface, detachment of this complex, exposure of fresh surfaces by fragmentation, etching etc.

Varadachari *et al*. (1994) observed that whereas olivine and biotite were extensively

***Corresponding Author Email :** kghoshcu@gmail.com

fragmented by organic acid weathering, tourmaline and microcline were not significantly fragmented. Hornblede grain showed the formation of a new crystalline phase at the surface. Microcline dissolution proceeded with the dissolution of ultrafine particles that were present at the surface of the grain; there was also etching and pitting of the surface (Varadachari *et al.*, 1994). Price *et al.* (2005) observed etch pits on epidote surface in the parent rocks of weathered regolith. Weathered feldspars of the glacial till soils studied by SEM showed the development and growth of etch pits (Mermut *et al.*,1986).

Wollast (1967) reported that silicate dissolution resulted in the formation of a leached layer. The thickness of this amorphous layer on feldspar weathered by slightly alkaline groundwater was estimated by SEM to be 10 nm (Zhu *et al.*, 2006). However, Lee *et al.* (2007) using combined fluorescence and TEM (transmission electron microscopy) found no evidence of amorphous or crystalline weathering products immediately beneath the surface of naturally weathered feldspars but observed etch pits at grain surface. This is in agreement with Velbel's hypothesis (1993) which states that protective surface layers cannot form on major rock forming silicates like feldspars, pyroxenes, amphiboles and olivines and instead etch pits formed by interface-controlled reactions are ubiquitous. Harshly etched structures were also observed in the SE micrographs of H_2SO_4 leached olivine (Seyama *et al.*, 1996). XRD and SEM/EDS analyses showed weathering in biotite to commence from the edges followed by exfoliation towards the interior (Young, 1998).

Literature on surface alteration of primary minerals by HAs appears to be limited. Here in this study, we investigated the changes in surface features of primary silicates by treatment with HA. The same set of minerals studied here, were earlier used for studies on alterations by small molecular weight organic acids (Barman *et al.*, 1992; Varadachari *et al.*, 1994). We have used both petrographic microscope and scanning electron microscope to observe surface alterations of olivine (nesosilicate), epidote (sorosilicate), tourmaline (cyclosilicate), hornblende (inosilicate), biotite (phyllosilicate) and microcline (tectosilicate). Results reveal the striking differences in behaviour between the different types of silicates and also the differences in weathering by HAs as compared to small molecular weight organic acids.

Materials and Methods

The silicate minerals were provided by the Geological Survey of India, Kolkata. They were powdered and dry-sieved to obtain the 80-150 mesh size fraction, washed with water and dried in an oven at 80°C and were characterized chemically and by XRD. These minerals were described in detail by Das *et al.* (2013, 2014a, 2014b).

Humic acid (HA) was extracted from the surface soil (0-15 cm) of an Alfisol (Ultic Paleustalf, ferruginous soil; Vishnupur, W. Bengal). The method of extraction, fractionation, purification and characterization of HA was carried out as described by Das *et al.* (2013).

Chemical analysis of the minerals reported earlier (Das *et al.*, 2013, 2014a, 2014b) were as follows : Olivine 40.45% SiO_2, 7.08% FeO + Fe_2O_3, 3.26% CaO and 47.67% MgO; epidote 44.46% SiO_2, 11.11% FeO + Fe_2O_3, 21.79% Al_2O_3, 21.30 CaO and 1.54% MgO; tourmaline 40.98% SiO_2, 11.45% FeO + Fe_2O_3, 33.81% Al_2O_3, 1.35% Na_2O and 8.59% B_2O_3; hornblende 43.66% SiO_2, 13.19% FeO + Fe_2O_3 , 13.89% Al_2O_3, 14.00% CaO and 11.19% MgO; biotite 35.94% SiO_2, 24.90% FeO + Fe_2O_3, 18.16% Al_2O_3, 3.17% TiO_2, 5.31% MgO and 10.41% K_2O; microcline 71.25% SiO_2, 16.83% Al_2O_3 and 11.32% K_2O. Major XRD bands for olivine were 7.33, 3.91, 3.75, 2.77, 2.16, 2.03 Å, for epidote, 5.08, 4.28, 3.35, 3.15, 2.46, 2.17, 2.03, 1.64 and 1.28 Å, for

tourmaline, 6.35, 4.62, 4.23, 3.47, 2.95, 2.31, 2.12, 1.87 and 1.59 Å, for hornblende, 8.4, 3.13, 2.6 and 2.03 Å, for biotite 10.04, 3.35 and 2.51 Å and for microcline 10.13, 6.56, 4.25, 3.86, 3.73, 3.5, 3.39, 3.26 and 2.04 Å. The data indicated that the silicate samples were quite typical of their own group.

The analytical characteristics of the HA sample was described earlier (Das *et al.*, 2013). Briefly, the elemental analysis data of the Alfisol HA on dry ash-free basis was 54.90% C, 6.51% H, 5.64% N and 32.95% O. The E_4/E_6 ratio of the HA was 3.27, the NaOH titratable acidity was 260 cmol kg^{-1} and the total acidity was 666 cmol kg^{-1}. IR spectrum of the HA showed absorptions at 3750, 3400, 2900 2370, 1600, 1200, 1000, 660 cm^{-1}.

The silicate minerals were treated with the HA in the following manner (Das *et al.*, 2013) : 2 g mineral was taken in a plastic bottle and 50 mL of 1000 ppm HA at pH 7 was added to it. Agitated on a shaker intermittently (5h/day) for three consecutive months and the residue was filtered, washed and finally dried at 80°C.

The minerals and their weathered products were mounted on glass slides and photographed under a James-Swift petrographic microscope in normal light and with crossed polarizers, at 10X. For SEM studies, representative samples mounted on aluminium stubs were coated with carbon and gold-palladium. Micrographs were recorded on a Hitachi S-2360N operating at 18 kV.

Results and Discussion

Petrographic microscopic studies with olivine, epidote and tourmaline are presented in Fig. 1.

Unweathered olivine under normal light (Fig. 1a) shows dispersion of colors under cross polarized light (Fig. 1b). Dark patches attributed to precipitation of cation-HA complex on the surface of weathered olivine grains imply that these regions are opaque (Fig. 1c) and do not show any birefringence under polarized light (Fig. 1d). Therefore, the dark patches do not exhibit

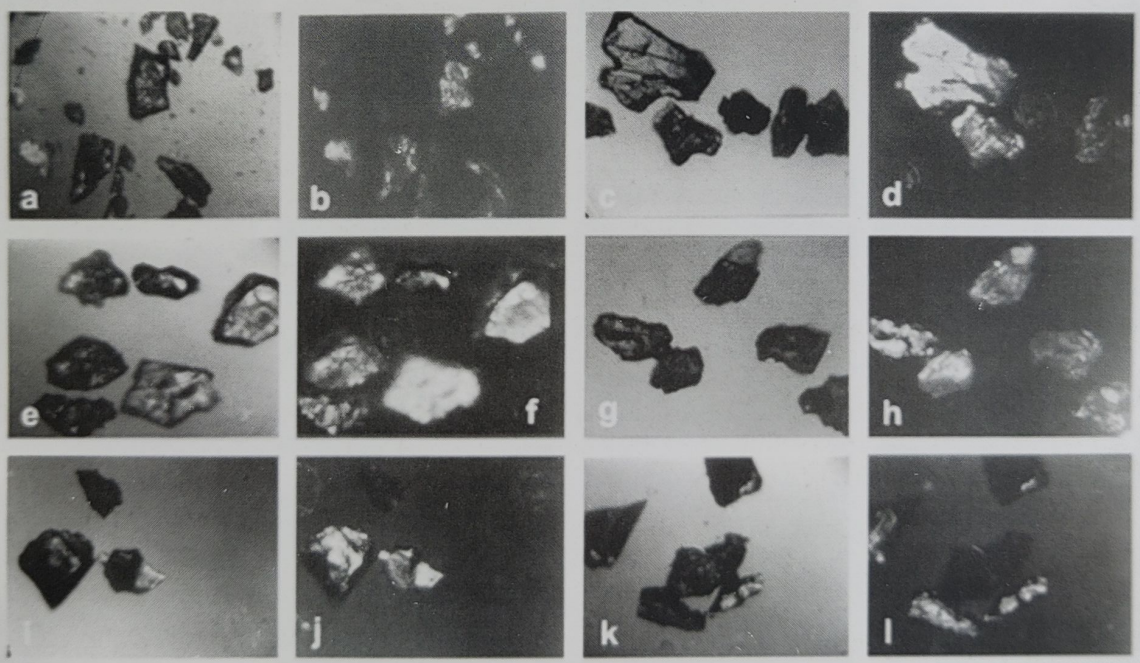

Fig. 1. *Petrographic micrographs : [A] under normal light : (a) olivine, (e) epidote, (i) tourmaline, (c) weathered olivine, (g) weathered epidote, (k) weathered tourmaline, [B] under cross polarized light : (b) olivine, (f) epidote, (j) tourmaline, (d) weathered olivine, (h) weathered epidote, (l) weathered tourmaline.*

crystallinity. Unweathered epidote under normal light (Fig. 1e) shows strong birefringent colors under polarized light (Fig. 1f). With weathered epidote, black surface deposits attributed to the presence of HA can also be seen (Fig. 1g), as with olivine. These regions are rendered amorphous; strong birefringence is absent in the weathered residues, only small regions of the mineral surface remain in tact to show birefringence (Fig. 1h). Tourmaline reveals significant changes caused by deposition of HA on the grain surface making them totally amorphous (Fig. 1k); only small points of birefringence are observed under polarized light (Fig. 1l). Unweathered tourmaline under normal light (Fig. 1i) exhibits birefringence under cross polarizers (Fig. 1j).

In Fig. 2, unweathered hornblende (Fig. 2a) shows strong birefringent colors (Fig. 2b). The weathered mineral shows frayed edges with prominence of dark deposits of HA rendering them partially non-crystalline (Fig. 2c) with reduction in colors (Fig. 2d) indicating surface damage. The unweathered biotite (Fig. 2i) and its weathered residue could not be photographed under polarized light as the mineral in itself shows low birefringence. The sheets look essentially the same even after treatment although numerous small dark particles can be seen (Fig. 2j) which are attributed to HA deposits. Biotite has been altered the least in complete contrast to the drastic changes suffered by tourmaline. Microcline originally (Fig. 2e) shows low birefringence (Fig. 2f). Dark deposits of HA on microcline, though less than on other minerals, are evident on the surface of the weathered grains rendering those regions non-crystalline (Fig. 2g); this has further been confirmed by the nearly absent birefringence under cross polarized light (Fig. 2h). The appearance of the unreacted mineral after weathering (Fig. 2g) indicates that only minor changes are brought about.

Scanning electron microscopy shows that the minerals have undergone significant changes (Fig. 3, 4 and 5).

SEM of the original (unweathered) olivine

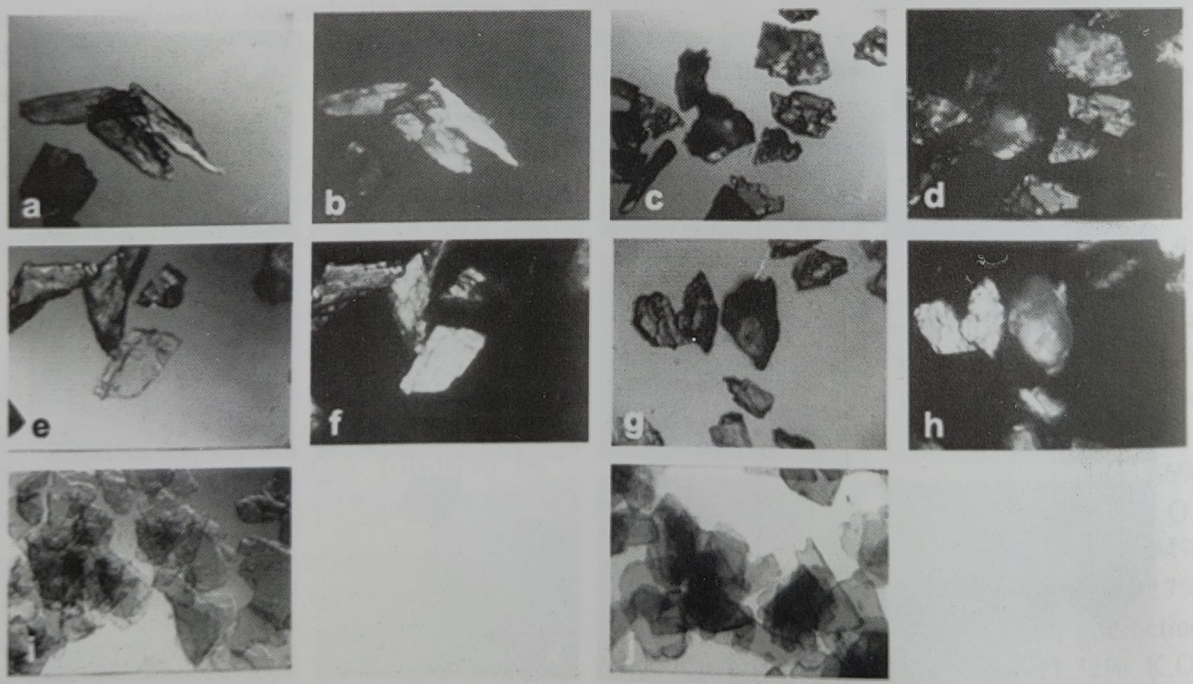

Fig. 2. *Petrographic micrographs : [A] under normal light : (a) hornblende, (e) microcline, (i) biotite (c) weathered hornblende, (g) weathered microcline, (j) weathered biotite, [B] under cross polarized light : (b) hornblende, (f) microcline, (d) weathered hornblende, (h) weathered microcline.*

surface is seen in Fig. 3a and b. Fig. 3a shows prismatic faces on one of the surfaces of olivine; in Fig. 3b, part of the unweathered olivine edge is seen. Weathered olivine surfaces are shown in Fig. 3 c-f. The effect of surface etching is prominent in Fig. 3c, leading to the formation of ridges and furrows. Pitting is observed in Fig. 3d which result in edge fissure. In Fig. 3e, pits are observed with deposition of material in its periphery. Indications of transfer of material between certain regions of the grain are observed in Fig. 3f which presents alternate lighter and darker patches.

Clean surfaces of epidote grain are shown in Fig. 3g and h. In the weathered residue (Fig. 3i), the surface has become frosted with the development of pits; fine grains of fine material also appear to be deposited. Fig. 3j portrays a highly etched surface of epidote grain. Three sets of cleavages have been accentuated by etching; Fig. 3k shows the development of multiple pits along with fine powdery deposition in and around the etch pits. Evidence of HA deposition from SEM studies is in Fig. 3l where a set of step fractures caused by breakage show deposits of HA within the cracks.

Plain and clean surface of unweathered tourmaline is evident in Fig. 4a and b. Fig. 4b shows conchoidal fracture on the grain surface. After treatment with HA, the edges have become frayed leading etching (Fig. 4c). The opening up of cleavage planes due to leaching and the development of triangular pits in their junction are observed in Fig. 4d. Etch pits have been opened up in Fig. 4e and numerous small particles are evident in Fig. 4f that shows the edges after weathering.

In unweathered hornblende, a strong set of cleavages on a clean rhombic surface are evidenced in Fig. 4g and h; the edges appear clean and sharp. HA treatment has greatly changed the surface features of hornblende. On the whole, the surface with broad patterns of etch pits are prominent from Fig. 4i. A comparison between Fig. 4h and j suggests that weathering has deepened the edges. Deep

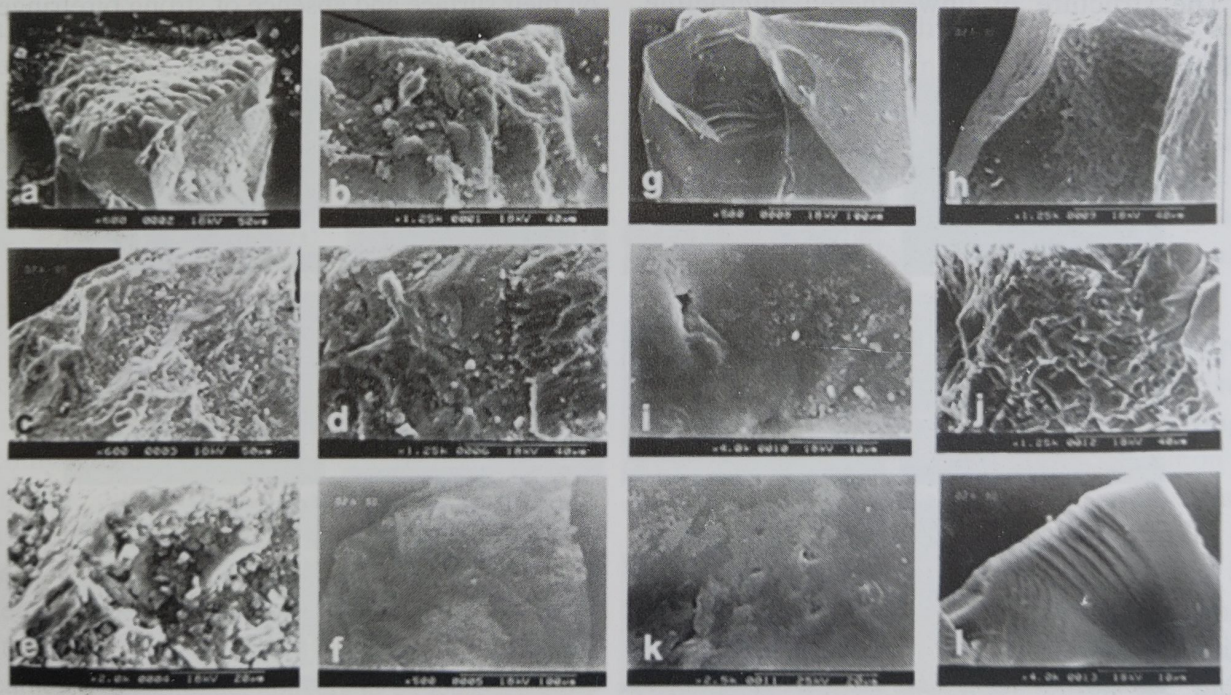

Fig 3. *Scanning electron micrographs (a) (b) olivine, (c) (d) (e) (f) weathered olivine, (g) (h) epidote, (i) (j) (k) (l) weathered epidote.*

crevices are formed close to and parallel to the cleavage planes. Frayed edges of cleavage surface with deposition of fine powdery material in the interspace is observed in Fig. 4k. Distinct coating with development of small pits having upper surface covered with a layer of fine material is evident in Fig. 4l. Some of the pits here are triangular in shape; the LHS part of the photograph shows a grain with these features at lower magnification and the RHS at higher magnification.

Biotite shows much less alterations due to weathering by HA. The surface of unreacted biotite flakes is shown in Fig. 5a and the edges in Fig. 5b. Effect of etching of weathered biotite is observed in Fig. 5c which shows peeling off of edges. Shearing and warping of the edges are seen in Fig. 5d, at both lower (LHS) and higher (RHS) magnifications. A distinct region bordering the tri-junction of edges in Fig. 5e may be due to depletion of certain constituents; Fig. 5f shows a slight opening up of layers and blunting of sharp edges of biotite after treatment with HA.

The structure of unweathered microcline grains are seen in Fig. 5g and h; Fig. 5h shows edges with the presence of microparticles on the surface. Microcline has also undergone fairly substantial changes. The etched surface of microcline has created cavities as seen in Fig. 5i while distinct pits are observed on the surface of weathered microcline in Fig. 5j and at different layers as in Fig. 5k; the edges have developed deep lines and are frayed (Fig. 5l).

Conclusions

In continuation of our previous work on the dissolution of silicate minerals by HAs, we investigated changes in surface morphology after reaction. In all, six minerals were studied representing the major silicate groups starting from sorosilicates (olivine) to the tectosilicate (microcline). Petrographic study revealed the deposition of HAs on the surface of mineral grains. The regions of HA deposition lost their crystallinity and did not show birefringence under polarized light. Olivine and epidote showed considerable changes with dark patches of HA on their surface and absence of strong birefringent

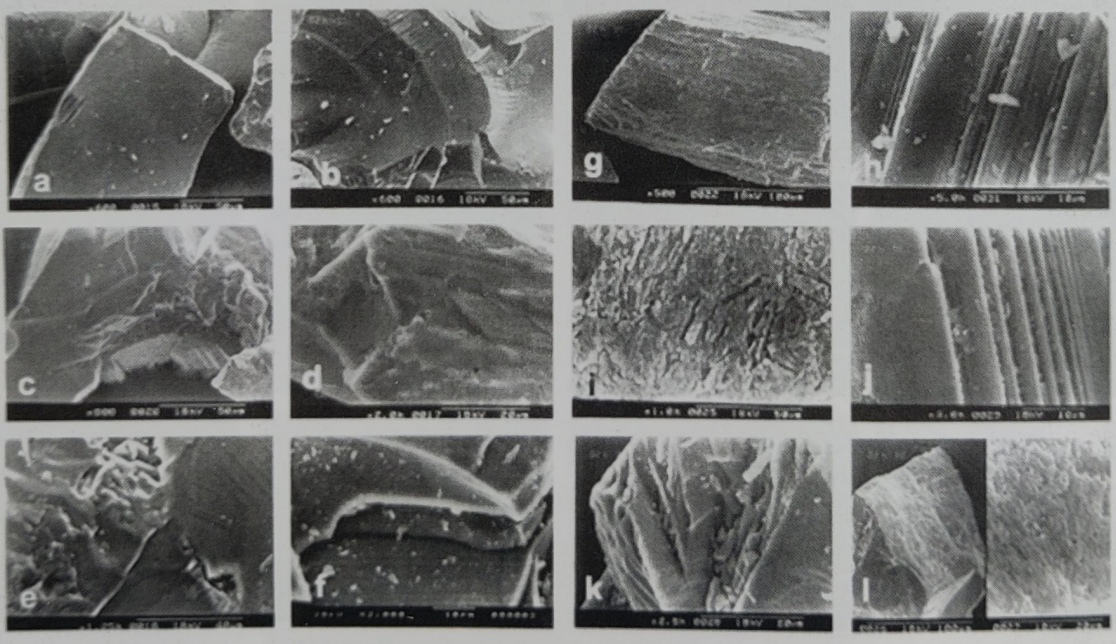

Fig. 4. *Scanning electron micrographs (a) (b) tourmaline, (c) (d) (e) (f) weathered tourmaline, (g) (h) hornblende, (i) (j) (k) (l) weathered hornblende.*

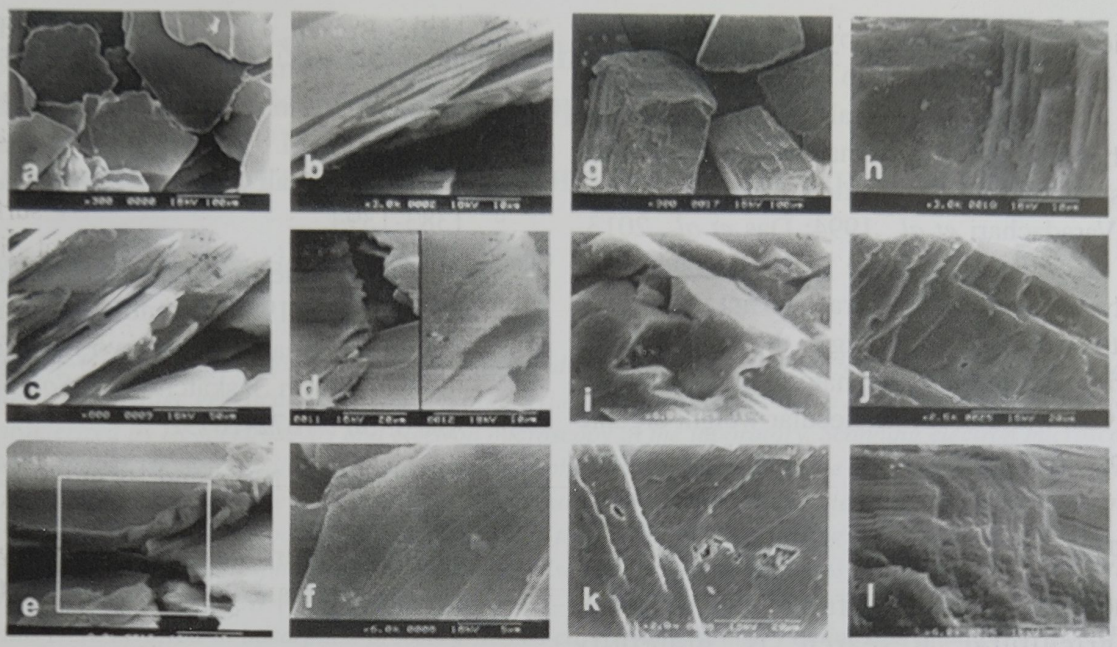

Fig. 5. *Scanning electron micrographs (a) (b) biotite, (c) (d) (e) (f) weathered biotite, (g) (h) microcline, (i) (j) (k) (l) weathered microcline.*

colors. Unexpectedly, tourmaline also showed significant changes, with much of the surface being rendered non-crystalline. Hornblende was transformed to partially amorphous surface with frayed edges indicating surface damage. The sheets of biotite looked essentially the same even after weathering although a large number of small dark particles could be seen. Microcline alteration was not visible, although a few dark deposits of HA could be seen.

Scanning electron microscopy showed that the surfaces of the minerals changed significantly. In weathered olivine, surface etching and prominent pitting were observed. Weathered epidote also showed surface with pitting and etching as well as the deposition of fine material withinthe pitted edges. Unexpectedly, tourmaline residue suffer significant changes to its surface due to weathering. It's edges are frayed, surface is etched and has large number of pits together with deposition of fine particles. In contrast, weathered hornblende, appears to be least affected by HA. The biotite layers are mostly intact and there is only a slight fraying and opening of edges. This is in contrast to the observations of Varadachari *et al.*, (1994); on weathering with small organic acids, biotite layers were substantially openend up. Those studies also showed that tourmaline and microcline were scarcely affected by small organic acids and SEM could not reveal any pitting or etching. Here, both tourmaline and microcline appear to have been significantly weathered by humic acid with evidence of distinct pitting and etching and fraying of edges. Deposition of material is also evident.

The microscope studies of weathered products lead proof to our previous inference from dissolution kinetics that crest-trough behaviour of dissolution is due to deposition of insoluble metal-humate complexes at the surface of the mineral. This study also suggests an interesting fact that weathering of silicates by HAs affects the minerals differently than small molecular weight organic acids. Minerals like tourmaline and microcline, which are quite resistant to water or organic acid weathering actually suffer significant breakdown and

alterations when weathered by HA, wheras biotite which is quite susceptible to organic acids is one of the most resistant minerals on weathering by HA. These results, in combination with our earlier studies on silicate dissolution (Barman *et al.*, 1992; Varadachari *et al.*, 1994; Das *et al.*, 2013, 2014a &b) clearly indicate that the concept of stability sequence of minerals is not unique; it needs to be revised according to the environment, primarily considering the nature of weathering agent, viz., water or low molecular weight organic acids or humic acids.

Acknowledgements

The funding received from Indian Council of Agricultural Research is gratefully acknowledged. The authors are also grateful to Dr. J.S. Roy and Mr. Sekhar Ghosh, Department of Geology, University of Calcutta, Kolkata for technical help.

References

Barman, A.K., Varadachari, C. and Ghosh, K. 1992. Weathering of silicate minerals by organic acids. I. Nature of cation solubilisation. *Geoderma* **53**: 45-63.

Das, S., Ghosh, K. and Varadachari, C. 2013. Weathering of silicate minerals by humic acids : I. Nature of cation solubilisation from olivine and tourmaline and characteristics of the residual products. *Clay Res.* **32** : 58-75.

Das, S., Ghosh, K. and Varadachari, C. 2014a. Weathering of silicate minerals by humic acids : II. Nature of cation solubilisation from hornblende and biotite and characteristics of the residual products. *Clay Res.* **33** : 46-63.

Das, S., Ghosh, K. and Varadachari, C. 2014b. Weathering of silicate minerals by humic acids : III. Nature of cation solubilisation from epidote and tourmaline and characteristics of the residual products. *Clay Res.* **33** : 110-125.

Lee, M.R., Brown, D.J., Smith, C.L., Hodson, M.E., Mac Kenzie, M. and Hellman, R. 2007. Characterization of mineral surfaces using FIB and TEM : A case study of naturally weathered alkali feldspars. *Am. Miner.* **92** : 1383-1394.

Mermut, A.R., Ghebre-Egziabhier, K. and St. Arnaud, R.J. 1986. Quantitative evaluation of feldspar weathering in two Boralfs (Gray Luvisols) from Saskatchewan. *Soil Sci. Soc. Am. J.* **50 :** 1072-1079.

Price, J.R., Velbel, M.A. and Patino, L.C. 2005. Allanite and epidote weathering at the Coweeta hydrologic laboratory, western North Carolina, U.S.A. *Am. Miner.* **90 :** 101-114.

Seyama, H., Soma, M. and Tanaka, A. 1996. Surface characterization of acid-leached olivines by X-ray photoelectron spectroscopy. *Chem. Geol.* **129** : 209-216.

Varadachari, C., Barman, A. K. and Ghosh, K. 1994. Weathering of silicate minerals by organic acids. II. Nature of residual products. *Geoderma* **61**: 251-268.

Velbel, M. A. 1993. Formation of protective surface layers during silicate-mineral weathering under well-leached oxidizing conditions. *Am. Miner.* **78** : 405-414.

Wollast, R. 1967. Kinetics of the alteration of K-feldspar in buffered solutions at low temperature. *Geochim. Cosmochim. Acta* **31 :** 635 - 648.

Young, J.G. 1998. Vermicular kaolinite epitactic on primary phyllosilicates in the weathering profiles of anorthosite. *Clays Clay Miner.* **46:** 509-520.

Zhu, C., Veblen, D.R., Blum, A.E. and Chipera, S.J. 2006. Naturally weathered feldspar surfaces in the Navajo sandstone aquifer, Black Mesa, Arizona : Electron microscopic characterization. *Geochim. Cosmochim. Acta* **70**: 4600-4616.

(Received August 2016; Accepted October 2016)

Clay Research, Vol. 34, No. 2, pp. 99-109 (2015)

Characterization of Nanoclay-phosphatase Complex with IR Spectroscopy and Electron Microscopy

RANJAN PAUL, S.C. DATTA, K.M. MANJAIAH AND R. BHATTACHARYYA

Division of Soil Science and Agricultural Chemistry, IARI

Abstract–*Commercial phosphatase enzyme (acid and alkaline) was immobilized with different nanoclays collected from three genetically different soil orders (i.e. Inceptisol, Vertisol and Alfisol) and complexes were characterized by IR spectroscopy and electron microscopy in the laboratory. Scanning electron microscopy (SEM) images showed modification of surface morphologies of nanoclay due to phosphatase adsorption (appearance of boulder like structures and rough surfaces after immobilization). IR scanning confirmed presence of characteristic band of clay mineral due to H-O-H, Si-O stretching and Al-O-H bending in all nanoclays. Nanoclay-phosphatase complexes were also characterized by means of IR and it was found that carbonyl (C=O) amide III (–CO-N–) and amide I (–CO-NH_2) group present in various amino acid side chains were involved in adsorption process whereas carboxylate, primary amine and amide II (–CO-NH–) groups present in glutamine became more free on adsorption.*

Introduction

Soil enzymes have very high affinity for soil colloids. These can easily be immobilized in soils and do not remain free in solution. Their release and bioactivity in the adsorbed phase depend largely on soil enzyme complex. Extent of adsorption will depend upon the type of the colloid and the structure of the enzyme (shape, size and functional group). Phosphatase is very common and important in the biogeochemical cycle in soil which catalyses the conversion of organic phosphorus substrates into inorganic form (Allison, 2006). Adsorption and activity of phosphatase were considerably influenced by several minerals and clay fractions present in soil (Dick and Tabatabai, 1987; Huang *et al.,* 1995; Rao *et al.,* 1996). Clays having at least one dimension in less than 100 nm range are referred to nanoclays (Calabi *et al.,* 2009). Because of their nano dimensions these nanoclays are superior in terms of specific surface area, CEC, surface charge density and surface reactivity than non-nano clay fraction. Due to very huge potential for agricultural, industrial and medicinal applications, nanomaterials have been the focus of much research during the past few decades (Holister *et al.,* 2003). Nanoclays are an important entity of natural nanomaterials that are present in the soil system. Naturally occurring nanosize fraction of clays is short range ordered non-crystalline material like allophane consisting of spherical particles with a diameter of 3.5-5 nm, present in all soils and abundant in volcanic andisols (Calabi *et al.,* 2012). These short range ordered minerals can interact with phosphatase, bring conformational change in it (Tarafdar *et al.,* 1988) and greatly influence its activity upon adsorption (Rao *et al.,* 1996).

Studies have been done on the adsorption of phosphatase on nanoclays and allophanic material isolated from volcanic origin soils (Calabi *et al.,* 2012). But reports regarding characterization of pure phosphatase and its complexes with nanoclays isolated from soils other than volcanic origin are scanty. Therefore the present investigation was undertaken to characterize

***Corresponding Author Email :** samar1953@yahoo.com

different types of nanoclay from Inceptisol, Vertisol and Alfisol (before and after removal of amorphous aluminosilicates) and their complexes with acid and alkaline phosphatase by infra-red spectrophotometry and scanning electron microscopy.

Materials and Methods

Chemicals

Acid Phosphatase (EC 3.1.3.2from potato, lyophilized powder, 6 unit per mg solid) and alkaline phosphatase (EC 3.1.3.1 from bovine intestinal mucosa, lyophilized powder 6-10 unit per mg solid) were purchased from Sigma (India). All other chemicals used were analytical grade from Merck.

Collection and preparation of soil samples

Soil samples from 0-15 cm depth were collected by following the standard procedure. The soils were from 3 major soil orders viz. Alfisol, Inceptisol and Vertisol from Purulia district (West Bengal), IARI farm and Bhopal respectively. The collected soil samples were air dried in shade, ground with the help of mortar and pestle, passed through a 2 mm sieve, weighed in new polythene packets in suitable amount and stored for further experimentation.

Nanoclay separation

Dispersion of clay (< 2μ) from Alfisol, Vertisol and Inceptisol was done by removing calcium carbonate, salts, organic matter and sesquioxides by treating with Sodium acetate pH 7, H_2O_2(Kunze, 1965) and citrate-bicarbonate-dithionate (DCB, Mehra and Jackson, 1960) respectively. To separate nano fraction the collected clay suspension was centrifuged at 5000 rpm for 3 minutes (Jackson, 1956) (calculated by using Stoke's Law average specification data of the Remi angular refrigerated centrifuge, C-24). Nano-fraction of clay remained in the supernatant which was then used for further analysis.

Separation of Amorphous aluminosilicates (Acid oxalate method under darkness)

Amorphous aluminosilicates(AM) from nanoclays were separated by treating with 0.2 M ammonium oxalate-oxalic acid buffer, pH 3.0 (Tamm reagent) and agitating for 4 hrs in darkness and mixture was decanted in a 50 mL centrifugation tube (Fey and Le Roux, 1977). It was then centrifuged to obtain clear supernatant solution. After adequate dilution, Si, Al and Fe were analyzed on supernatantby ICP - MS after destruction of oxalate matrix by boiling with concentrated nitric acid. Nanoclays remaining at the bottom of the centrifuge tube were washed multiple times with distilled water and used for phosphatase immobilization.

X-ray diffraction analysis

X-ray diffraction analysis of nanoclay samples (with and without amorphous aluminosilicates) was done following the standard methodology of Jackson (1956). For each clay sample four treatments were given, viz., (a) Mg-saturated - airdried, (b) K-saturated- air dried, (c) Mg-saturated and glycerol solvated and (d) K-saturated and heated to 5500C. Two mL of 2% suspension of nanoclay (with and without amorphous material) on 2.6 × 4.0 cm glass slide were then taken and then analyzed for powder XRD by using APD (Automated Powder Diffractometry) software in a Phillps PW 1729 X-ray diffractometer with the following settings of the instrument : Radiation type - CuKa; Generator voltage - 40 kV; Tube current - 20 mA; Scanning angle range - 3.0 to 30.002q; Scan step size:0.0102q; Scan type -Continuous; Scan speed time - 1.202q/min. Semi-quantification estimation was done from X-ray diffractograms of Mg-saturated and glycerol solvated samples following Gjems (1967) procedure. XRD characteristic and general characteristic of the nanoclays isolated from different soil aregiven in figure 1 and table 1.

Transmission electron microscopy (TEM)

For confirmation of nanoclays within nanometer range TEM images were taken. A 20 µl of aquous suspension of nanoclay was placed on carbon coated side of grid. After 1 min it was washed with 10-15 drops of distilled water and finally stained with 2% urinyl acetate. TEM images of dried grids were obtained with a JEOL 100 kb Microscope (JEOL 1011) at 120 kv.

Enzyme immobilization

Acid and alkaline phosphatase were immobilized on different nanoclay support (with and without amorphous aluminosilicates) following the procedure by Rao *et al.* (1996, 2000). 20 mg of the nanoclay was taken in a 2 mL vial and 30 µg of phosphatase protein in 1 ml of buffer were mixed. 0.1 M Na-acetate acetic acid buffer (pH 5) and 10 mMTris-Cl buffer (pH 8) were used for acid and alkaline phosphatase respectively. The mixtures were incubated at 30^0C for 1 hr and centrifuged at 10000 rpm for 10 min. The supernatants were removed and the pellets formed at the bottom of the tube were washed once with 0.1 M Na-acetate acetic acid buffer (pH 5). Then resuspended in equal volume of buffer, freeze dried in lyophilizer and stored in refrigerator (-10^0C) for further analysis.

Fourier Transmission infrared (FTIR) spectroscopy

Infrared spectroscopy of the powdered nanoclay (with and without AM), lyophilized pure phosphatase and phosphatase-nanoclay complex were carried out by using the Bruker: ALPHA, FTIR/ATR system (Typically 24 scans, Resolution- 4cm^{-1}). Samples were scanned in the region of 4000-400 cm^{-1}.

Scanning electron microscopy (SEM)

Scanning electron microscopy (SEM) studies of the powdered nanoclay samples (with and without AM) before and after enzyme immobilization were done with Zeiss EVOMA10 scanning electron microscope at 10.00 KV/EHT and 2.80-5.00×10^{-5} mbar between 200nm to 100µm after 24 nm palladium coating.

Results and Discussion

X-ray Diffraction

The X-ray diffraction pattern of Mg-saturated glycerol solvated nanoclay from an Inceptisol under preferred orientation showed peak at 2θ= 8.8^0 which corresponds to d-axis spacing of 1.01 nm (mica) (Fig 1). Another first order peak is also present at 2=12.2^0 with lesser intensity which corresponds to d-axis spacing of 0.711 nm. Therefore presence of mica (75%) and kaolinite (25%) was confirmed in inceptisol nanoclay. Similarly in Vertisol nanoclay smectite (89%) was present as dominant mineral with a small amount of kaolinite (11%). Alfisol nanoclay contained kaolinite(65%) as dominant mineral followed by mica (35%). The % content of different mineral present in all nanoclays are shown in table 1. Amorphous aluminosilicates content was found to be highest in nanoclay from Vertisol followed by inceptisol and alfisol (table 1)

Characterization of nanoclay-phosphatase complex by electron microscopy

Particle size of the nanoclay used for

Table 1. General characteristic of the nanoclays isolated from different soil.

Nanoclay type	Amorphous aluminosilicates (AM) content (%)	Clay mineral content (%)	Specific surface area (cm^2/g) by EGME method
Inceptisol Nano	8.62	Mica: 75 Kaolinite: 25	749
Vertisol Nano	11.95	Smectite: 89 Kaolinite: 11	894
Alfisol Nano	6.90	Kaolinite: 65 Mica: 35	369

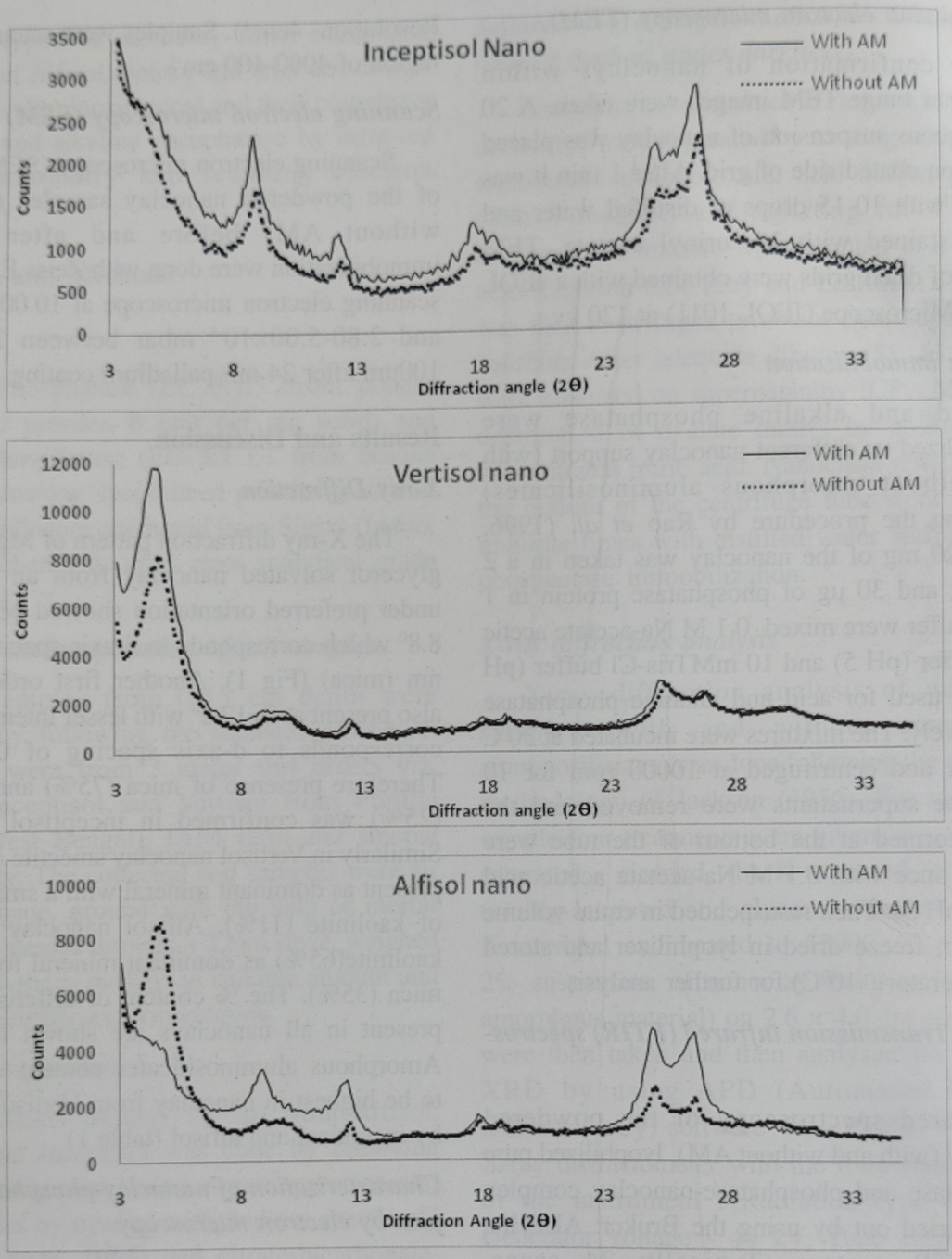

Fig. 1. *X- ray Diffractogram of Mg saturated glycerol solvated nanoclays isolated from different soils (with and without amorphous aluminosilicates)*

phosphatase immobilization was found to be in the nanoscale range (< 100 nm) as confirmed by TEM images (Fig 2). Nanoscale size was also observed after removal of amorphous aluminosilicates from all nanoclays. The surface morphologies of nanoclays was studied from SEM images (Fig 3). Presence of flaky and hexagonal type of structures in different nanoclays was indication of kaolinite, mica and smectite minerals, occurrence of which has been confirmed by XRD analysis results (table 1). The appearance of boulder like structures in nanoclay-

phosphatase complex might be due to the presence of enzyme and there was an aparant increase in particle size after immobilization (Rao *et al.*, 1996). Similar type of results were observed by Reshmi *et al.* (2013) in lipase immobilized montmorillonite. Rough surfaces of mineral after enzyme loading is due to deposition of protein in the form of enzyme which indicated aggregate formation (Assis *et al.*, 2003; Manocha *et al.*, 2008). Therefore enzyme immobilized nanoclay may be more tortuous than pure nanoclays (Yelkovan *et al.*, 2014).

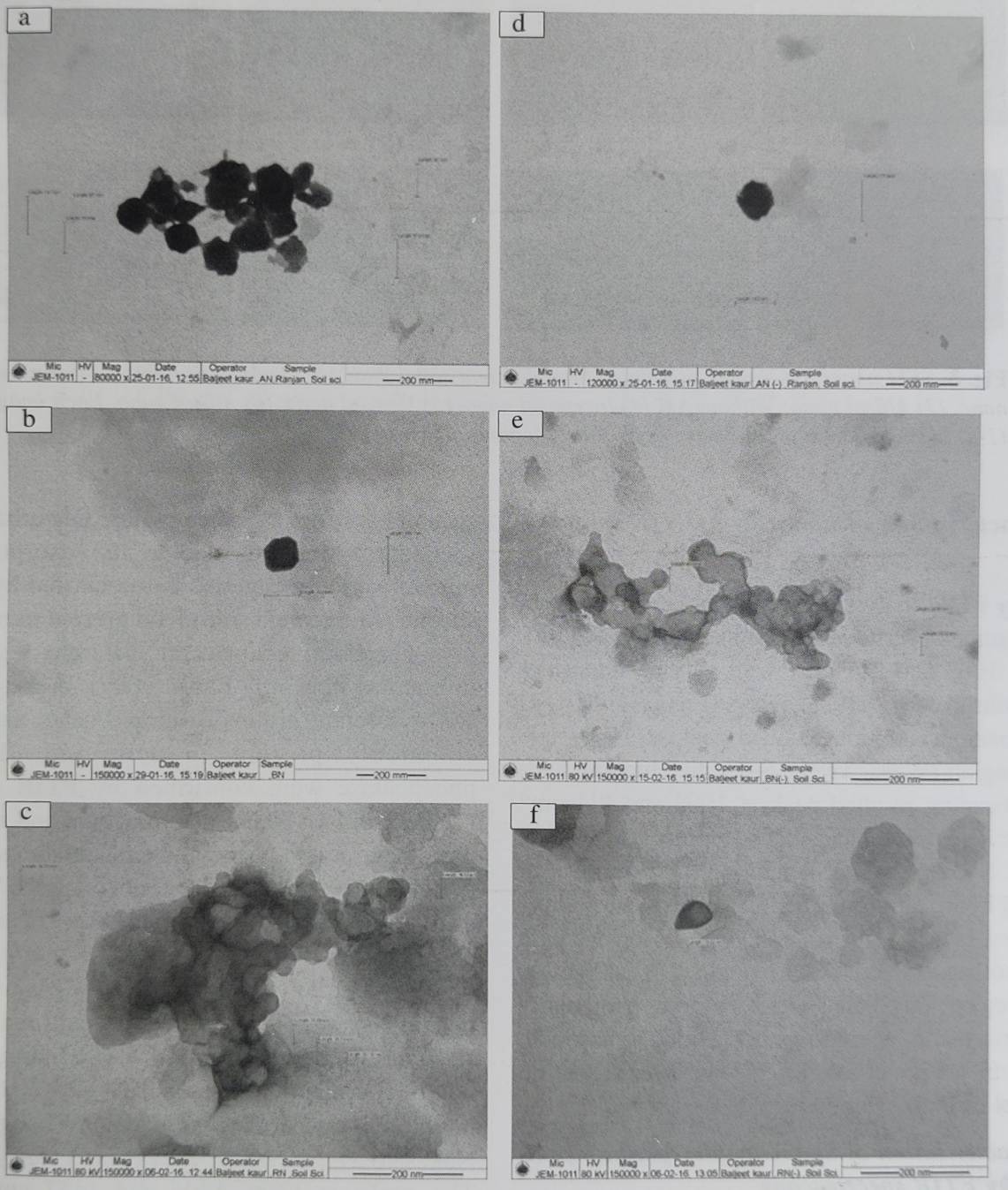

Fig. 2. *TEM images of Nanoclay isolated from different soils; With AM (a) Inceptisol nano, (b) Vertisol nano, (c) Alfisol nano, Without AM (a) Inceptisol nano, (b) Vertisol nano, (c) Alfisol nano*

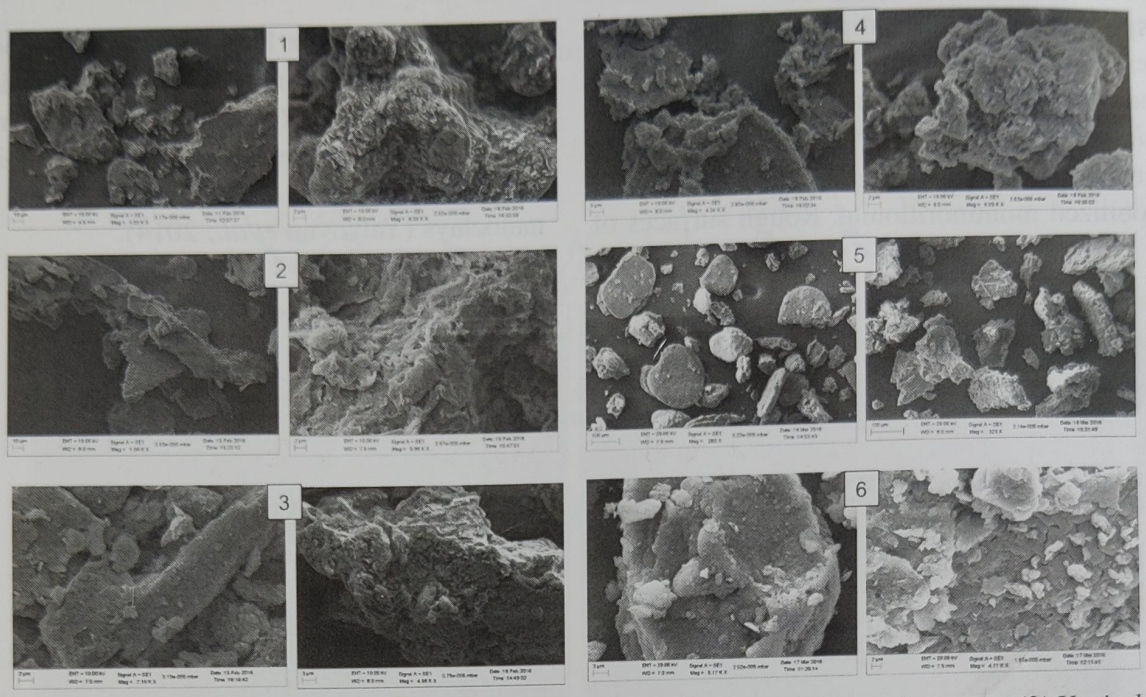

Fig. 3. *SEM images of Nanoclay isolated from different soils; With AM (1) Inceptisol nano, (2) Vertisol nano, (3) Alfisol nano; Without AM (4) Inceptisol nano, (5) Vertisol nano, (6) Alfisol nano. Each image (1-6) having without phosphatase (left) and with phosphatase (right)*

Characterization of nanoclay byFTIR spectroscopy

By FTIR analysis the functional groups present in the mineral surfaces were studied. Peaks at 1500-1600, 1003 and 911 cm^{-1} with varying intensities were observed for all nanoclays (Figure 4). H-O-H deformation vibration resulted peak at 1500-1600 cm^{-1} region (Wada, 1989). Si-O stretching and Al-O-H bending resulted peak at 1003 and 911 cm^{-1} respectively for all nanoclays (Farmer and Russel, 1964; He *et al.,* 1995; Abidin, 2007). Removal of amorphous aluminosilicates from nano clays resulted increase in transmittance (%) or decrease in absorbance at < 1100 cm^{-1} region. At 3400-3800 cm^{-1} region some bands were observed, particularly in Vertisol and Inceptisol nanoclay due to adsorbed water in surface or interlayer which was absent on Alfisol nanoclay (Farmer and Russel, 1964).

Characterization of nanoclay-phosphatase complex by FTIR spectroscopy

FTIR is also an important tool to determine secondary structure of enzymes. Disturbance in secondary structures due to its adsorption on mineral surfaces can also be monitored by FTIR spectra. Amino acid side chain present in proteins give characteristic peak at different region of infrared as shown by Barth (2007). In the present study different groups of amino acids that were commonly present in acid and alkaline phosphatase were confirmed by FTIR spectra (Table 2 and 3). FTIR spectra of acid and alkaline phosphatase demonstrated characteristic peaks of proteins appeared at wavenumbers of 1635, 1540 and 1574 cm^{-1}. These peaks were due to absorption by functional groups of amide I band (C=O stretching vibration), amide II band (N-H bending and C-N stretching modes), and amide III band (C-N stretching and N-H bending), with possible structures of–CO-NH_2, –CO-NH–, and/or –CO-N– respectively (Chen and Zhang, 2006; Nakasato *et al.,* 2004; Servagent *et al.,* 2000). The peaks at 1396, 1405 and 1457 cm^{-1} were associated with carboxyl and carboxylate groups.

Table 2. *Infra-red absorption bands (cm^{-1}) of pure acid phosphatase and its complexes with different nanoclay.*

Acid phosphatase enzyme	Nanoclay-acid phosphatase complexes						Assignments
	Inceptisol nano		Vertisol nano		Alfisol nano		
	With AM	Without AM	With AM	Without AM	With AM	Without AM	
619	620	617	619	620	620	620	C-H deformation (bend)
646	644	647	646	646	645	646	
801	800	801	802	800	806	806	C-H bend and ring pluckering
923	923	922	923	922	922	921	C-O stretch due to Serine
1013	1003	1008	1010	1001	1004	1003	C=O stretch (for carboxylic acids and drivatives) and C-N stretch
1068	Absent	Absent	Absent	Absent	Absent	Absent	
1405	1408	1418	1411	1416	1418	1417	C-O-H bending, carboxylate group of Glutamine
1574	1558	1569	1574	1569	1575	1575	C-N stretching and N-H bending (Amide III band) due to Aspartic acid, Tyrosine and Asparagine
2989	2996	Absent	2996	2995	2990	2991	O-H stretch (C-H overlap)
3156	3277	Absent	Absent	Absent	Absent	Absent	
3272	3156	Absent	Absent	Absent	Absent	Absent	
3418	3423	Absent	Absent	Absent	Absent	Absent	O-H stretch (H bonded)
3662	3648	3648	3648	3648	3648	3647	Free and intermolecular bonded O-H
3731	3734	3734	3732	3734	3731	3730	

Table 3. *Infra-red absorption bands (cm^{-1}) of pure alkaline phosphatase and its complexes with different nanoclay.*

Alkaline phosphatase enzyme	Nanoclay-alkaline phosphatase complexes						Assignments
	Inceptisol nano		Vertisol nano		Alfisol nano		
	With AM	Without AM	With AM	Without AM	With AM	Without AM	
614	662	662	662	662	663	662	C-H deformation (bend)
699	747	749	747	747	746	746	C-H deformation, 1^0 amine NH_2 scissoring (bend)
842	Absent	Absent	Absent	Absent	Absent	Absent	C-H bend, NH_2 scissoring and NH wagging, shift on H bonding
892	Absent	Absent	Absent	Absent	Absent	Absent	
963	908	908	909	908	908	908	C=O stretch from Serine
1059	997	994	Absent	998	998	998	C-N stretch, C=O stretch for carboxy lic acid and derivatives from Histidine and Threonine
1107	1032	Absent	1016	1016	1033	1033	
1280	1296	1296	1296	1296	1296	1296	C=O stretch from Serine
1396	1396	1396	1396	1396	1396	1396	C-O-H bend
1457	1457	1457	1457	1457	1458	1458	Carboxyl group
1540	1553	1553	1553	1553	1553	1553	N-H bend (Amide II) from Glutamine
1635	1627	1627	1627	1634	1628	1627	N-H bend (Amide I) from Arginine
2921	2969	2975	3975	2975	2976	2973	O-H stretch (H bonded), C-H overlap.

Peaks at 1013, 1059, 1068 and 1107 cm^{-1} were due to C=O and C-N stretching (Tarafdar *et al.,* 1988). Alkaline phosphatase showed band at 699 cm^{-1} due to 1^0 amine (Jackson and Mantsch, 1995). Peak showed at 2921, 2989, 3156, 3272 and 3418 cm^{-1} were due to O-H stretching. Peaks observed at 600-800 cm^{-1} range were due to C-H bending vibration. The presence of peaks corresponding to wavenumbers similar to free enzymes were also observed in nanoclays after enzyme immobilization but peak position either shifted to higher/lower frequency, remain in same position or absent. Shifting of 614, 699, 1280, 1405 1540 and 2921 cm^{-1} frequencies to the higher value in all nanoclays suggest that functional group present in these regions did not take part in adsorption and became more free as reported by Mortland (1966) and Tarafdar *et al.* (1988). In the contrary shifting of 963, 1013, 1059, 1107, 1574, 1635 and 3662 cm^{-1} frequencies to lower values in all nanoclays indicates that these functional groups are involved in adsorption of enzyme molecules to the mineral surface as reported previously by Tarafdar *et al.* (1988). Peaks at 619, 646, 801,923, 1396 and 1457 cm^{-1} remained at same position as these functional groups were not involved in adsorption process. Peaks showed by pure enzymes at 842, 892, 1068 and 3000-3400 cm^{-1} region were absent after its immobilization on different supports which demonstrated the decreases in α-helix structure and β-sheet of proteins, implying that secondary conformational changes in proteins occurred by adsorption on mineral surfaces (Quiquampoix and Burns,

2007; Servagent *et al.*, 2000).

Conclusion

Various functional group that were involved in the adsorption of acid phosphatase on different nanoclays were carbonyl (C=O) and Amide III (–CO-N–) present in amino acid side chain of aspartic acid, tyrosine and asparagine, free and intermolecular bonded OH. Whereas carbonyl group of serine, histidine and threonine and amide I group of arginine present in alkaline

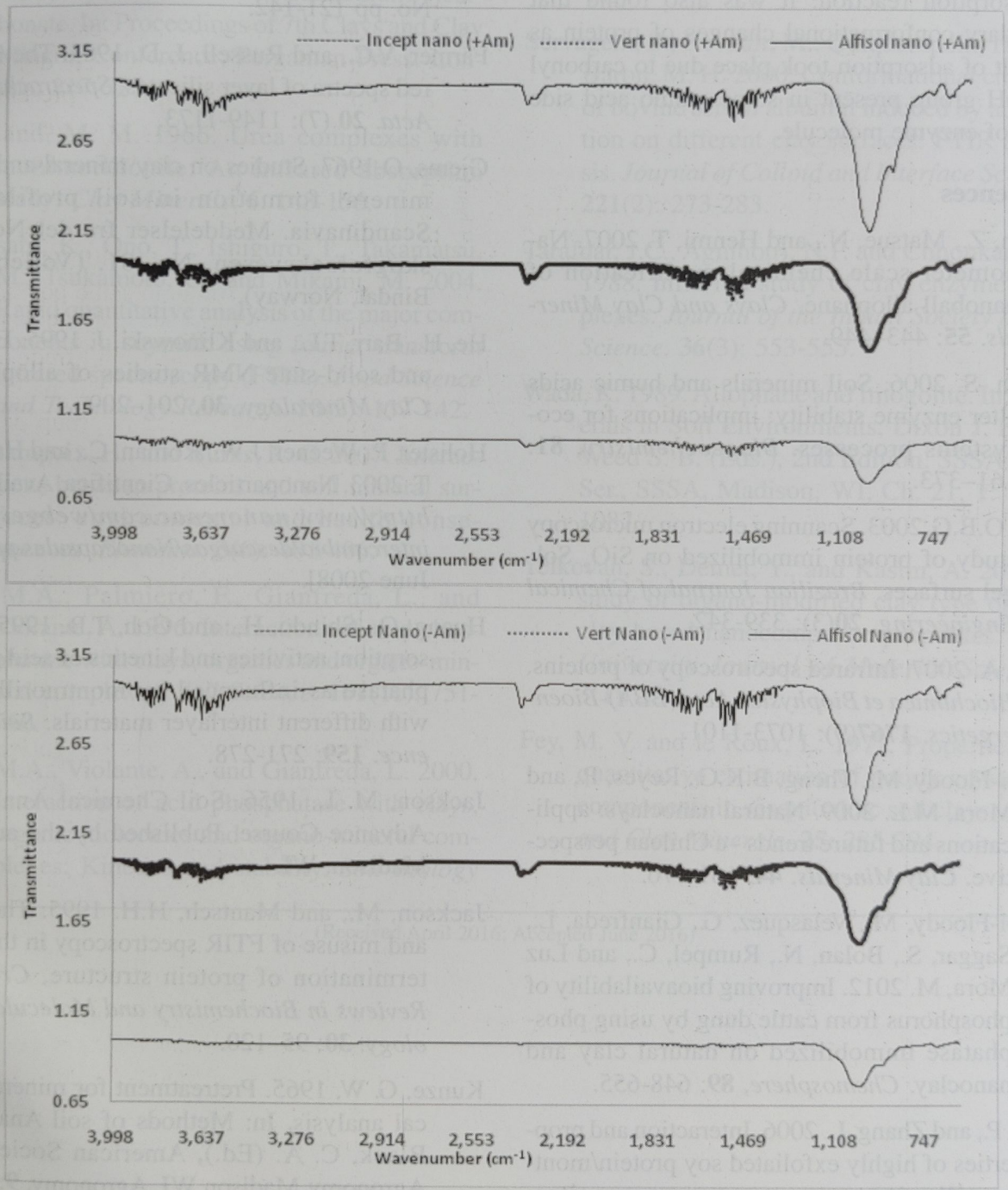

Fig. 4. *Comparison of FTIR spectra of different nanoclay isolated from Inceptisol, Vertisol and Alfisol (with and without AM).*

phosphatase were involved in adsorption. The functional group that became more free on adsorption were carboxylate (acid phosphatase), primary amine and amide II (alkaline phosphatase) group present in glutamine. C-H group present in all the enzymes doesn't involved in adsorption reaction. It was also found that secondary conformational changes of protein as a result of adsorption took place due to carbonyl and OH group present in some amino acid side chain of enzyme molecule.

References

Abidin, Z., Matsue, N., and Henmi, T. 2007. Nanometer-scale chemical modification of nanoball allophane. *Clays and Clay Minerals*. **55**: 443–449.

Allison, S. 2006. Soil minerals and humic acids alter enzyme stability: implications for ecosystems processes. *Biogeochemistry*, **81**: 161–373.

Assis, O.B.G. 2003. Scanning electron microscopy study of protein immobilized on SiO_2 Sol-gel surfaces. *Brazilian Journal of Chemical Engineering*. **20**(3): 339-342.

Barth, A. 2007. Infrared spectroscopy of proteins. *Biochimica et Biophysica Acta (BBA)-Bioenergetics*. **1767**(9): 1073-1101.

Calabi-Floody, M., Theng, B.K.G., Reyes, P., and Mora, M.L. 2009. Natural nanoclays: applications and future trends - a Chilean perspective. *Clay Minerals*. **44**: 161-176.

Calabi-Floody, M., Velasquez, G., Gianfreda, L., Saggar, S., Bolan, N., Rumpel, C., and Luz Mora, M. 2012. Improving bioavailability of phosphorus from cattle dung by using phosphatase immobilized on natural clay and nanoclay. *Chemosphere*, **89**: 648-655.

Chen, P., and Zhang, L. 2006. Interaction and properties of highly exfoliated soy protein/montmorillonite nanocomposites. *Biomacromolecules*. **7**(6): 1700-1706.

Dick, W.A. and Tabatabai, M.A. 1987. Kinetics and activities of phosphatase-day complexes. *Soil Science*. **143**: 5-15.

Farmer, V. C., and Russell, J. D. 1966. Infrared absorption spectrometry in clay studies. *Clays and Clay Minerals*. Conference Proc. No. pp 121-142.

Farmer, V.C., and Russell, J. D. 1964. The infrared spectra of layer silicates. *Spectrochimica Acta*. **20** (7): 1149-1173.

Gjems, O.1967. Studies on clay mineral and clay mineral formation in soil profiles in Scandinavia. Meddelelser fra det Norske skogforsoksvesen. No. 81. (Vollebekk: Bindal, Norway).

He, H., Barr, T.L., and Klinowski, J. 1995. ESCA and solid-state NMR studies of allophane. *Clay Mineralogy*. **30**, 201–209.

Holister, P., Weener, J.W., Roman, C., and Harper, T. 2003. Nanoparticles. Cientifica. Available: *http://www.nanorenac.com/webgestion/intercambio/descargas/Nanocapsules.pdf* [11 June 2008].

Huang, Q., Shindo, H., and Goh, T.B. 1995. Adsorption, activities and kinetics of acid phosphatase as influenced by montmorillonite with different interlayer materials. *Soil Science*. **159**: 271-278.

Jackson, M. L. 1956. Soil Chemical Analysis-Advance Course. Published by the author, Madison, WI.

Jackson, M., and Mantsch, H.H. 1995. The use and misuse of FTIR spectroscopy in the determination of protein structure, *Critical Reviews in Biochemistry and Molecular Biology*. **30**: 95–120.

Kunze, G. W. 1965. Pretreatment for mineralogical analysis. In: Methods of soil Analysis. Black, C. A. (Ed.), American Society of Agronomy Madison WI. Agronomy, **9**: 210-221.

Manocha, S., Patel, Nikesh., and Manocha, L. M. 2008. Development and characterization of nanoclays from Indian clays. *Defence Science Journal.* **58**(4): 517.

Mehra, O. P. and Jackson, M. L. 1960. Iron oxide removal from soils and clays by dithionite-citrate systems buffered with sodium bicarbonate. In: Proceedings of 7th Clays and Clay Mineral Conference; Pergaman Press: London, 317-327.

Mortland, M. M. 1966. Urea complexes with montmorillonite: An infrared absorption study: *Clay Minerals*. **6**: 143-156.

Nakasato, K., Ono, T., Ishiguro, T., Takamatsu, M., Tsukamoto, C., and Mikami, M. 2004. Rapid quantitative analysis of the major components in soymilk using fourier transform infrared spectroscopy (FTIR). *Food Science and Technology Research.* **10**(2): 137-142.

Quiquampoix, H., and Burns, R. G. 2007. Interactions between proteins and soil mineral surfaces: environmental and health consequences. *Elements*. **3**(6): 401-406.

Rao, M.A., Palmiero, F., Gianfreda, L., and Violante, A. 1996. Interactions of acid phosphatase with clays, organics and organo-mineral complexes. *Soil Science*. **161**(11): 751-760.

Rao, M.A., Violante, A., and Gianfreda, L. 2000. Interaction of acid phosphatase with clays, organic molecules and organo-mineral complexes: Kinetics and stability. *Soil Biology and Biochemistry*. **32**:1007–1014.

Reshmi, R., and Sugunan, S. 2013. Superior activities of lipase immobilized on pure and hydrophobic clay supports: Characterization and catalytic activity studies. *Journal of Molecular Catalysis B: Enzymatic*. **97**: 36-44.

Servagent, S., Revault, M., Quiquampoix, H., and Baron, M. H. 2000. Conformational changes of bovine serum albumin induced by adsorption on different clay surfaces: FTIR analysis. *Journal of Colloid and Interface Science*. **221**(2): 273-283.

Tarafdar, J.C., Agnihotri, N.P. and Chhonkar, P.K. 1988. Infra-red study of clay enzyme complexes. *Journal of the Indian Society of Soil Science*. **36**(3): 553-555.

Wada, K. 1989. Allophane and Imogolite. In: Minerals in Soil Environments, Dixon J. B. and Weed S. B. (Eds.), 2nd Edition. SSSA Book Ser., SSSA, Madison, WI, Ch. 21, 1: 1051-1087.

Yelkovan, S., Demet, Y., and Kasim, A. 2014. A study of organo-modified clay type on pet-clay based nanocomposite properties. *Usak University Journal of Material Sciences*. 3(1): 33.

Fey, M. V. and le Roux, L. 1977. Properties and quantitative estimation of poorly crystalline components in sesquioxidic soil clays. *Clays and Clay Minerals*. **25**: 285-294.

(Received April 2016; Accepted June 2016)

ACKNOWLEDGEMENT

I grate fully acknowledge the help received from the followings scientists /Professors who reviewed the manuscripts for 2015 issue

1. Dr Padikkal Chandran
2. Dr Sanjay Ray
3. Dr Goutam Goswami
4. Dr Siddhartha Mukhopadhyay
5. Dr K.M Manjaiah

INSTRUCTIONS FOR CONTRIBUTORS

CLAY RESEARCH is the official publication ofTHE CLAY MINERALS SOCIETY OF INDIA and is published twice a year, in June and December. The Journal undertakes to publish articles of interest to the international community of clay scientists, and will cover the subject areas of mineralogy, geology and geochemistry, crystallography, physical and colloid chemistry, physics, ceramics, civil and petroleum engineering and soil science.

The Journal is reviewed in *Chemical Abstracts, MineralogicalAbstracts, and Soils and Fertilizers.*

Paper (in English) should be submitted to the Editor, Clay Research **"The Clay Minerals Society of India"** Division of Soil Science and Agricultural Chemistry, I.A.R.I., New Delhi-I to 012. E-mail: samar_I953@yahoo.com. At least one of the authors should be member of THE CLAY MINERALS SOCIETY OF INDIA. Submission is an undertaking that the manuscript has not been published or submitted for publication elsewhere.

Manuscripts should not exceed sixteen typed (double spaced) pages including tables and illustrations. **The original and two copies oftext and illustrations should be submitted.**

Form Manusciprts should be typewritten, double spaced on white paper, with wide margins. Intending contributors should consult a recent issue of CLAY RESEARCH for the standard format and style. The manuscript should have the sections ABSTRACT, introductory portion (untitled), MATERIALS AND METHODS, RESULTS and DISCUSSION and REFERENCES.

Title page should contain manuscript title, full name(s) of author(s), address (es) of the institution(s) of the author(s), a short running title not exceeding 60 characters including spaces, footnotes if any to the title, and complete mailing address of the person to whom communications should be sent.

Abstract should be a condensation of the ideas and results of the paper. It should not exceed 25'0 words. Do not make reference to the literature in the abstract.

Tables should have the simplest possible column headings. Type each table on a separate page; indicate location in the text by marking in the margin of text page.

Figures should be self-illustrative, drawn with black India ink on tracing paper or white Board. The lattering should be large enough to permit size reduction to one Journal page column width (about 7.0 cm) without sacrificing legibility. **The original tracing should be submitted**. The size of the drawing should not exceed 24 × 17 cm. Give the numbered legend on a separate sheet, not on the figure itself. Data available in the tables should not be duplicated in the form of illustrations. Indicate the location of the figure in the text by marking in the margin of the page.

Photographs should be in the form of glossy prints with strong contrast. In photomicrographs, the scale in micron or other suitable unit should be drawn on the print. Give the numbered legend on a separate sheet. Indicate the location of the photograph in the text by making in the margin of the text page.

References should be cited in the text by the name(s) of author(s) if two or less, and year of publication. If there are more than two authors, give the name ofthe first author followed by *'et al'* and year. Full references giving author(s) and initial(s), year, title of paper, (journal, volume, number if paged separately), first and last pages should be listed alphabetically at the end of the paper. Journal title should be abbreviated in accordance with the World List of Scientific Periodicals and its sequences. Examples are

Grim, R.E., Bray, R.H. and Bradley, W.R. 1937. The mica in argillaceous sediments. *Am. Miner.* **22**:813-829.

Brindley, G.W. 1961. Chlorite minerals. In *(G.* Brown, Ed.) *The X-ray Identification and Crystal Structures of Clay Minerals,* Mineralogical Society, London, pp.242-296.

Theng, B.K.G. 1974. *The Chemistry of Clay Organic Reactions,* Adam. Hilger, London, 343 pp.

Review Every manuscript submitted to CLAY RESEARCH is independently reviewed by one or more referees. Acceptance or rejection of a manuscript is the responsibility of the Editor.

Reprints No free reprints are supplied to authors. Order for priced reprints should be sent when required by the Editor.

Clay Research

Vol. 34 **December 2015** **No. 2**

CONTENTS

Printed at : Cambridge Printing Works, New Delhi-1100028. (Mobile : 9811860113)